Delft University of Technology
Faculty of Applied Sciences
Laboratory of Materials Science

Influence of Heat Treatment on the Fracture Toughness of AA6061 and AA6061 mmc

Graduate report

A.C. van Gorp

Supervisor: ir K.M. Mussert
Delft, June 1999

SAMENVATTING

Metaal matrix composieten (mmcs) zijn materialen met een metalen matrix en een versterking van bijvoorbeeld keramiek. Metaal matrix composieten worden gebruikt omdat ze bijzondere eigenschappen kunnen combineren, bijvoorbeeld de goede vervormbaarheid van aluminium met de hogere sterkte van keramiek. In dit onderzoek wordt een deeltjes versterkt aluminium matrix composiet gebruikt, de matrix is AA6061 en de versterking is 20 vol.% hoekige Al_2O_3 deeltjes met een gemiddelde grootte van 20 μm.
Het doel van dit onderzoek was om de invloed van verschillende precipitaten op de breuktaaiheid van AA6061 aluminium en AA6061 versterkt met 20 vol.% Al_2O_3 deeltjes te bepalen.

In standaard warmtebehandelingen, zoals bijvoorbeeld de veel gebruikte T6 warmtebehandeling, ontstaat een mix van verschillende precipitaten. Om maar één soort precipitaat te krijgen is een andere manier van warmtebehandelen gebruikt, gebaseerd op een DSC curve van het materiaal. In deze manier van warmtebehandelen wordt eerst oplosgegloeid gedurende 2 uur op 530°C, gevolgd door afschrikken in koud water. Daarna wordt met 5°C/min opgewarmd tot na een specifieke piek in de DSC curve, gevolgd door afschrikken in koud water. Er wordt vanuit gegaan dat dan alleen precipitaten aanwezig zijn die in de laatste piek gevormd zijn.
Er zijn trekproeven gedaan aan AA6061 proefstukken in de verschillende warmtebehandelingscondities, om de invloed van de verschillende precipitaten op de sterkte en de versteviging te bepalen.
De parameter om de breuktaaiheid van een materiaal weer te geven is de K_{Ic}. Er is een ASTM standaard voor het bepalen van de K_{Ic}. In dit onderzoek wordt de standaard disk-shaped compact tension proefstuk geometrie gebruikt. In eerste instantie werden proefstukken met een rechte notch gebruikt voor AA6061. Dit leidde tot ongeldige waarden en voor de volgende proeven aan AA6061 en het AA6061 mmc zijn daarom proefstukken met een chevron notch gebruikt.

Eén van de twee alternatieve warmtebehandelingen leidt tot hogere sterkte, de andere leidt tot lagere sterkte dan in de aangeleverde T651 conditie.
Er zijn voor AA6061 geen geldige K_{Ic} waardes gevonden doordat tunnelling optrad en het vermoeiingsscheurfront scheef was.
Voor het AA6061 mmc is slechts één geldige K_{Ic} waarde gemeten door problemen tijdens het voorvermoeien. De scheur was namelijk niet te zien tijdens het voorvermoeien hetgeen leidde tot breuk tijdens het voorvermoeien of het stoppen van voorvermoeien bij een te korte vermoeiingsscheur. Er is in dit onderzoek een manier ontwikkeld om tijdens het voorvermoeien de scheurlengte te berekenen uit de compliantie verandering van het proefstuk.
Het is onmogelijk om met de licht microscoop verschillen in de microstructuur na verschillende warmtebehandelingen wat betreft de precipitaten te zien. Wel is duidelijk zichtbaar dat de korrels in proefstukken die een warmtebehandeling gekregen hebben na levering in T651 conditie veel groter zijn loodrecht op de extrusie richting dan de proefstukken in de aangeleverde T651 conditie. Dit betekent dat er korrelgroei optreedt tijdens het oplosgloeien. Deze grotere korrels in de in het laboratorium warmtebehandelde condities kunnen een oorzaak zijn voor de afschuivingsbreuk in de trekstaafjes.

SUMMARY

Metal matrix composites (mmcs) are materials with a metal matrix combined with reinforcement usually ceramic. Metal matrix composites are used because they can combine properties like a good formability of aluminium and a high strength of ceramic. In this research a particle reinforced aluminium matrix composite is used. The matrix consists of AA6061 and the reinforcement consists of 20 vol.% angular Al_2O_3 particles with an average size of 20μm.
The aim of this research was to determine the influence of different precipitates on the fracture toughness of AA6061 and AA6061 reinforced with 20 vol.% Al_2O_3 particles.

In standard heat treatments, like the often-used T6 heat treatment, a mixture of different precipitates forms during heat treatment. To obtain only one kind of precipitate a different way of heat treatment was used. This different kind of heat treatment was based on a DSC trace of the material. First the material is solutionized for 2 hrs at 530°C, followed by water quenching, like in standard heat treatments. After this the specimens are heated at a speed of 5°C/min until the end of a DSC trace peak is reached then the specimens are immediately water quenched. It is assumed that only the precipitates that are formed during the last DSC peak before quenching have formed are present in the material.
Tensile tests on AA6061 specimens in the different heat treatment conditions are performed to determine the influence of the different precipitates on the strength and the strain hardening of AA6061.
The parameter used to measure the fracture toughness of a material is K_{Ic}. An ASTM standard is used to determine the K_{Ic}. In this research the disk-shaped compact tension specimen is used. At first specimens of AA6061 with a straight through notch were tested, but that led to invalid K_{Ic} values. Therefore the other specimens had chevron notches.

One of the alternative heat treatments led to higher strength, the other led to lower strength than the delivered T651 condition.
None of the measured K_Q values of AA6061 is a valid K_{Ic}. This because the fatigue precrack was tunnelled and oblique.
From the K_Q values of the AA6061 mmc, only one is a valid K_{Ic}. During fatigue precracking the AA6061 mmc material, the fatigue crack was not visible. Therefore specimens broke during fatigue precracking or fatigue precracking was stopped too early, before the required precrack length was reached. During this investigation a way to calculate the fatigue crack length during fatigue precracking from the measured compliance was developed.
It is impossible to discern the different precipitates after the different heat treatments with the light microscope. But it is clear that the grains in the heat treated specimens were larger perpendicular to the extrusion direction than the grains in the delivered T651 condition were. This indicates that grain growth occurs during solutionizing. The larger grains in the heat treated specimens might explain the shear fracture of the tensile specimens.

CONTENTS

1. INTRODUCTION

A metal matrix composite (mmc) is a material which consists of particles, whiskers or fibres embedded in a metallic matrix. The basic assumption behind the use of a composite material is the extent to which the qualities of two or more distinct constituents can be combined without seriously accentuating their shortcomings. Mmc material is used to construct in lighter and stronger materials.
In this research an mmc with an AA6061 matrix and 20 vol.% Al_2O_3 particles is investigated. The research is concentrated on the fracture toughness and heat treatment of the mmc and matrix material.

The aim of this research is measuring the K_{Ic} of AA6061 and AA6061 with 20 vol.% Al_2O_3 particles and the influence of heat treatment on the K_{Ic}. Three different heat treatments are compared to see which one leads to higher fracture toughness values in AA6061 20 vol.% Al_2O_3 mmc.

In chapter 2 the theoretical background of metal matrix composites, the applied heat treatments and the critical stress intensity factor are described. The next chapter deals with the experimental parts of this research.
To keep the results conveniently arranged, the results of measurements on AA6061 and AA6061 with 20 vol.% Al_2O_3 particles are listed in chapter 4 and 5 respectively. Discussion on the results and the tests can be found in chapter 6, followed by conclusions in chapter 7. The last chapter gives some recommendations for further research.

This research was conducted as a graduating project to obtain a master's degree in Materials Science at Delft University of Technology. It is part of a PhD project that focuses on the mechanical properties, and finite element modelling of discontinuous mmcs.

2. THEORY

2.1 Metal Matrix Composites

The term metal matrix composite (mmc) encompasses a wide range of scales and microstructures. Common to them all is a continuous metallic matrix. The reinforcing phase is usually a ceramic and can be continuous (fibres), or discontinuous (particles and whiskers), see figure 2.1.

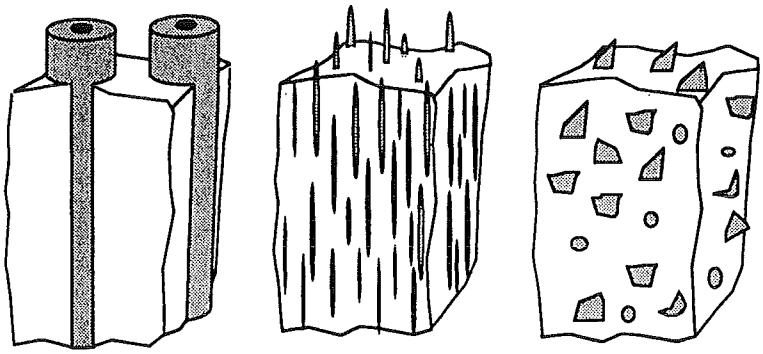

Figure 2.1: Schematic depiction of the three types of mmcs, classified according to the type of reinforcement [1]

The high formability of the matrix makes it possible that mmc material can be formed or shaped after production, which is not the case for the older polymeric matrix composites (pmcs) [1]. The freedom to separate material preparation and component production procedures, in much the same as with unreinforced metals, presents both an opportunity and a potential pitfall.
Dependent on the reinforcing constituent, pmcs as well as mmcs are anisotropic. But unlike aligned polymer-based composites, excellent axial performance can be combined with transverse properties that are more than satisfactory in mmcs.

The first mmc like materials extensively researched were the dispersion and precipitation hardened metal systems. For both dispersion and precipitation hardening, the basis of the strengthening mechanism is to impede dislocation motion (Orowan inhibition) with small particles. The small particles are fine oxide particles or non-shearable precipitates. The spacing between the small particles should be minimised to obtain higher strengths. The matrix bears the applied load.
In the 1960s mmcs were developed with a copper or aluminium matrix and boron or tungsten fibres. In these composites with high reinforcement fractions (40-80%), the role of the matrix is primarily to transmit and distribute the applied load to the fibres.
In the 1980s discontinuously reinforced mmcs were developed. In these mmcs both matrix and reinforcement bear substantial proportions of the load. The particles in these materials do not play an important role in Orowan inhibition of dislocation motion; they are loaded as in continuous reinforced systems. However, unlike continuously reinforced systems, the matrix strength, which is affected by precipitation and dislocation strengthening, also plays an important role.
The stress can vary sharply from point to point, but at force equilibrium the external load must equal the sum of the volume-averaged loads borne by the constituents, see equation 2.1 [1].

$$(1-f)\overline{\sigma}_M + f\overline{\sigma}_R = \sigma_E \quad (2.1)$$

where: f is the volume fraction of reinforcement
$\overline{\sigma}_M$ is the volume averaged matrix stress
$\overline{\sigma}_R$ is the volume averaged reinforcement stress
σ_E is the external stress

The reinforcement is usually stiffer and stronger than the matrix so it is beneficial for the stiffness and strength of the mmc if the reinforcement bears a large part of the external load, see equation 2.1.

Different materials are suitable as matrix materials, but aluminium matrix composites are the most frequently used and investigated mmcs. The matrix of an mmc can consist of different types of aluminium alloys, heat treatable as well as non-heat treatable. The matrix used in this investigation is AA6061, a heat treatable aluminium alloy with mainly Mg and Si as alloying elements.
Frequently used ceramic reinforcements are SiC and Al_2O_3. In this research the ceramic reinforcement consists of Al_2O_3 particles.

The mechanical properties of mmcs can be influenced by the particle size and volume fraction of the reinforcing particles or the heat treatment condition of the matrix [2]. The following sections deal with these parameters.

2.1.1 Particle Size and Fracture Toughness

In literature, there is no consensus whether the fracture toughness of mmcs increases or decreases with particle size.
According to Mortensen [3] the influence of reinforcement size can be rationalised in fairly simple terms. The cracking material can be separated in a process zone where the material deforms in a highly inhomogeneous manner and the remainder of the material, which can be treated as a continuum. The plastic zone can now be defined as the region where plastic deformation of the composite can be accounted for by treating the composite as a continuum, and the remaining cracked material in the immediate vicinity of the crack tip as the process zone.
The total fracture energy will scale proportionally to the process zone size, if all other conditions remain the same. When the reinforcement governs the process zone size, the total fracture energy will increase with increasing particle diameter. And the fracture toughness increases with the total fracture energy.
Another reason for the fracture toughness to increase with increasing particle diameter is the slight decrease in yield strength that arises when the diameter of the particles is increased. This effect is generally attributed to a reduced density of dislocations punched into the matrix by the particles upon cooling from process temperature [3]. A decrease in yield strength will increase the plastic zone size, according to equation 2.2 [3]:

$$r_p = C\frac{GE}{\sigma_y^2} \quad (2.2)$$

where: G is the total fracture energy per unit crack energy
E is the Young's modulus
C is a constant and is about 0.1 in plane strain and 0.3 in plane stress
σ_y is the yield stress

In some studies [4, 5], the fracture toughness decreases and the proportion of cracked particles increases above a certain particle diameter. The reason for this is that in larger particles internal flaws become large enough to weaken the ceramic material, decreasing the intrinsic crack resistance of the particles. This would lead to an optimum in particle size with regard to the fracture toughness.

Rabiei et al. [6] agree that larger particles crack with a cracking probability which increases as the particle size increases. However, they disagree that there is an optimum particle size, the smaller the particles the higher the fracture toughness [4, 6, 7], see table 2.1.

Table 2.1: K_{Ic} of AA6061 reinforced with 10 vol.% SiC particles of different sizes [6]

Particle size (μm)	K_{Ic} (MPa$\sqrt{m}$)
1	18.8-21
10	15.4-18
20	16.6-17.9

Other reports [3, 8] conclude that the influence of particle size on the K_{Ic} of mmcs is very small or negligible for particle sizes between 1 to 20 μm.

2.1.2 Volume Fraction and Fracture Toughness

Addition of ceramic particles to an aluminium matrix always decreases the fracture toughness. In literature there are several opinions about how the particle volume fraction can influence the K_{Ic}.
One opinion is that an increase in volume fraction of reinforcement causes a decrease in the fracture toughness [5, 6, 10]. This is caused by the fact that, when strain is the dominating factor for failure, the distance over which this strain should be accomplished (the distance between the particles) becomes shorter with increasing particle volume fraction. So the local strain in the matrix between the particles becomes higher and the matrix will fail sooner.
Other studies [8, 9] conclude that the volume fraction of reinforcement has no influence on the fracture toughness. These studies are in most cases reviewing studies comparing different studies and different materials. These different materials were produced in different ways and their mechanical properties should not be compared, because production conditions have a large influence on the mechanical properties [2].

2.2 Heat Treatment

Conventional heat treatments of aluminium alloys consist often of four steps. Step one is bringing the alloying elements into a saturated solid solution, this is done by heating the sample to a temperature in a single phase area of the phase diagram. In this research an Al-Mg-Si (0.4-0.8% Si and 0.8-1.2% Mg) alloy is investigated, of which a pseudo-binary Al-Mg_2Si diagram is shown in figure 2.2.

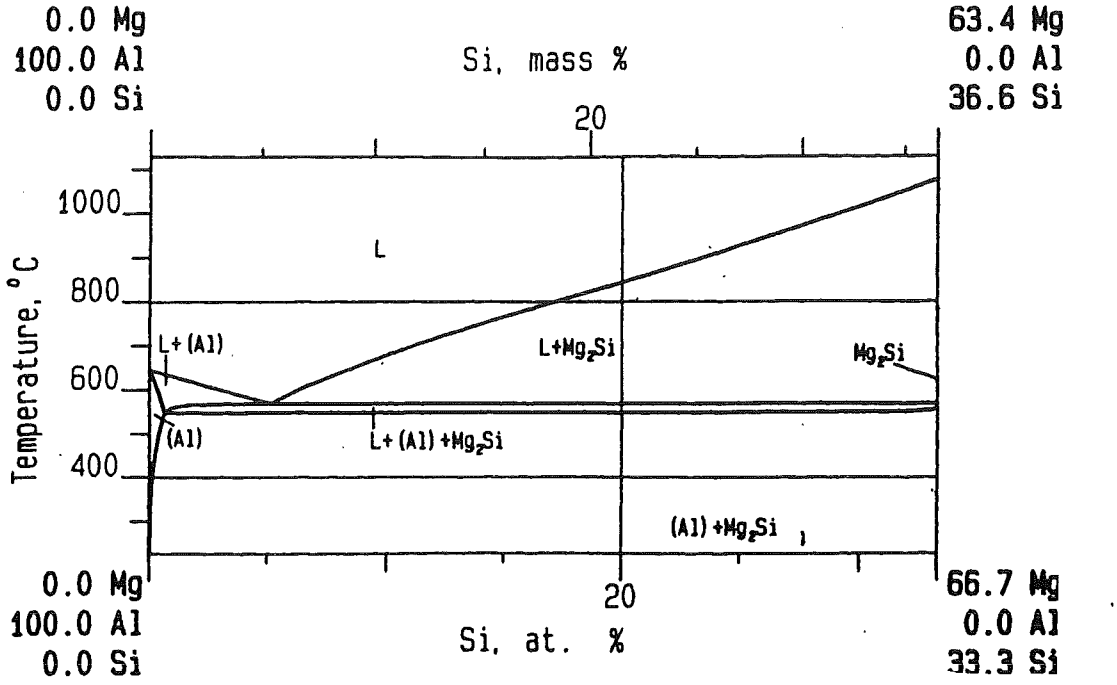

Figure 2.2: Pseudo-binary Al-Mg_2Si phase diagram [11]

A possible solution temperature for AA6061 alloys is 530 °C [12].
Step two is water quenching of the samples after this solution treatment, so as to keep the alloying elements in solid solution.
After water quenching the samples are heated again to a certain temperature at which the precipitates form, this is called artificial ageing. The material is kept at this temperature for a certain time. For example to obtain a T6, peak aged, condition in an AA6061 alloy the material is kept at 175 °C for 8 hours [12].
The final step is cooling down or quenching after artificial ageing.
Since different precipitates can form during artificial ageing, the precipitate structure is not known accurately after a conventional heat treatment.

Although the alloying elements in the AA6061 alloy and the mmc matrix material are both within the prescribed limits of AA6061 alloy composition, the response to heat treating can be somewhat different. The presence of reinforcing particles does not change the precipitation sequence for AA6061 as such, but it can accelerate some steps in the precipitation sequence or favour some precipitates over others. A possible acceleration is due to the higher dislocation density in the composite after quenching. These dislocations arise because of different thermal expansion coefficients of both matrix and reinforcing material [2].
The dislocations can act as nucleation sites for heterogene precipitation or act as diffusion paths. Depending on nucleation mode, heterogene or homogene, the nucleation of precipitates can be accelerated. If the growth of precipitates is controlled by the diffusion rate, if dislocation diffusion is dominant (at lower ageing temperatures) than the growth of precipitates is accelerated [13, 14, 15].
The higher dislocation density in the mmc can also retard some precipitation steps. For example at lower temperatures GP zone formation is retarded. For this, vacancies are supposed to play an important role. There is a lack of quenched-in vacancies in mmc material due to annihilation of vacancies with dislocations during quenching [16].

To avoid differences in precipitate structure and produce known and reproducible precipitate structures in the AA6061 material as well as the mmc matrix material, an

other heat treatment will be used in this study. The heat treatment used is derived from DSC traces of AA6061 material and mmc.

The Differential Scanning Calorimetry (DSC) technique is based on the difference in heat flow between the sample and a reference needed for a constant heating rate. There are separate containers for both sample and reference, and associated with each are individual heating elements as well as temperature measuring devices, see figure 2.3. Both cells are surrounded by a refrigerated medium that permits rapid cooling. The sample and reference chambers are heated equally into a temperature regime in which a transformation takes place within the sample. The temperature difference between the sample and the reference is kept zero by adding heat in one cell and reducing the heat input in the other cell. The amount of electrical energy per unit time which must be supplied to the heating elements (over and above the normal thermal schedule), in order to maintain the zero temperature difference, is assumed to be proportional to the heat released per unit time by the sample [17].

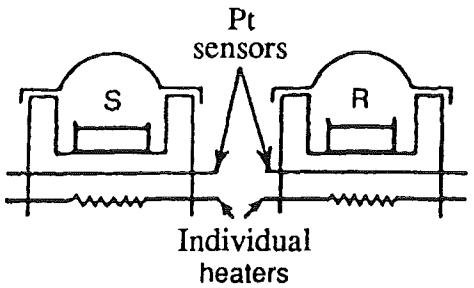

Figure 2.3: Schematic picture of a DSC [17]

Before testing the materials, a base line is recorded to account for the heating behaviour of the apparatus itself. The base line is composed by making a DSC run with two empty sample cup holders [18, 19].

A peak in the negative direction in a DSC trace is caused by an exothermic reaction and a peak in the positive direction is caused by an endothermic reaction. The peaks are a result of either the formation or solution of precipitates. From DSC traces in combination with precipitate identification, precipitation sequences can be deducted. In figure 2.4, the DSC traces of unreinforced AA6061 and AA6061 reinforced with 20 vol.% Al_2O_3 particles [18] are shown.

There are some reports about the precipitation sequence and kinetics in AA6061 alloys, but the exact order is not known as different results have been reported [2, 18, 19]. Since the materials used in the study of Chen et al. [18] are exactly the same as the materials used in this study, the results of that study will be used here.

The precipitation sequence as thought to be by Chen et al. [18] is as follows:
First during solutionizing the alloying elements go into a supersaturated solid solution. Than the sample is quenched. During subsequent heating, first vacancy related clusters are formed. In the DSC trace this is visible in the exothermic peak A.
The exothermic peak B is found to be a doublet and is due to the formation of GP-I and GP-II (or β") zones. These needle-shaped zones in the <100> direction are coherent or semi-coherent. These zones are very small and can be made visible through strain field contrast only.

Peak C overlaps peak B and is associated with formation of β', incoherent rod-shaped precipitates. The peaks after peak C are of the dissolution of the β' precipitates, the formation of the plate-like equilibrium β (Mg_2Si) precipitates (peak D) and melting of the sample [18, 20, 21].

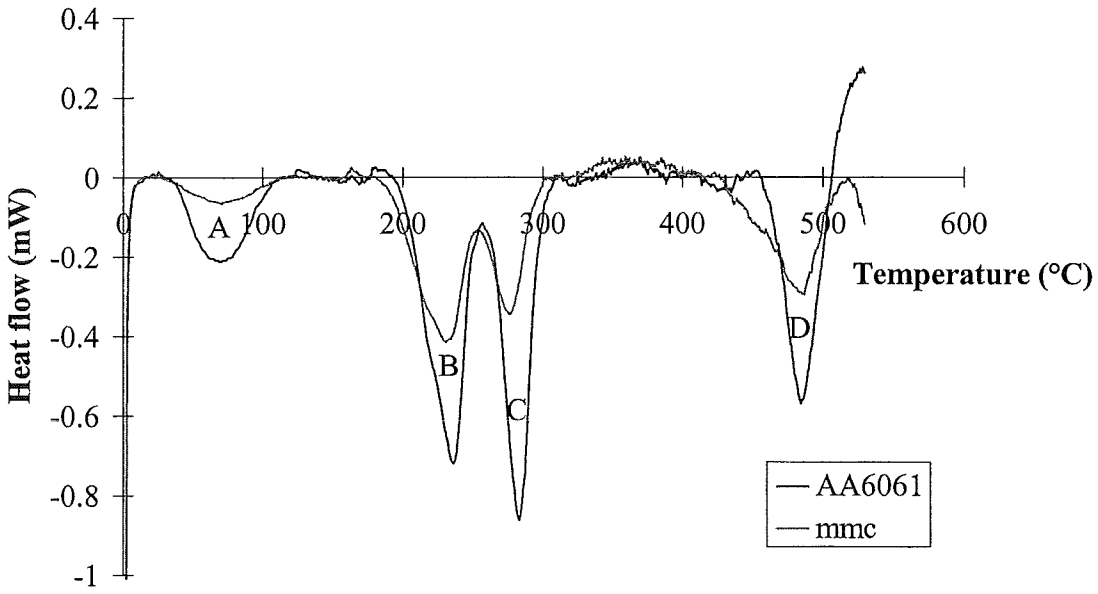

Figure 2.4: The DSC traces of AA6061 and the AA6061 with 20 vol.% Al_2O_3 particles, heating rate 5°C/min [18]

If the specimens used in this investigation, see section 3.4, are heated at the same rate as the DSC sample, it is assumed that the precipitation sequence is the same. So water quenching at the end of a peak in figure 2.4 should lead to reproducible precipitate structures that are similar for both the mmc and the base material.

2.3 The Critical Stress Intensity Factor

In the near vicinity of a discontinuity in materials, the stress is not evenly distributed, a stress intensity arises as a result of the discontinuity. This discontinuity is for example a crack. This stress intensity is denoted by the stress intensity factor, K. Using linear elastic theory the following expression can be found for the stress intensity factor in the vicinity of a crack tip [22]:

$$K = \sigma\sqrt{\pi a} \cdot f\left(\frac{a}{W}\right) \tag{2.3}$$

where: a is the crack length
σ is the applied stress
$f\left(\frac{a}{W}\right)$ is a geometry factor that differs for various specimen geometries

The applied stress can be in opening mode (mode I), sliding mode (mode II) or tearing mode (mode III) or a combination of these modes, see figure 2.5.

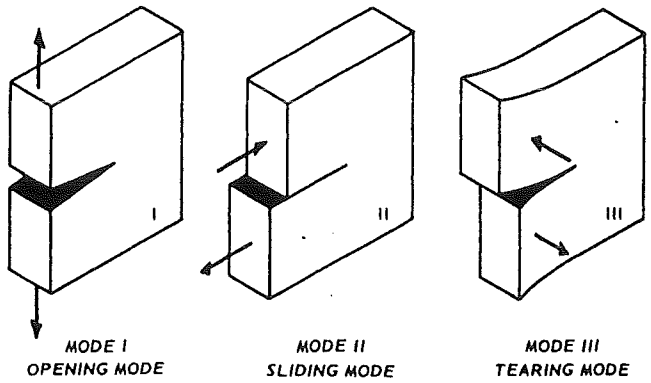

Figure 2.5: The three modes of loading [22]

Usually the stress mode is indicated by a subscript to K, K_I for example.
If the applied stress or the crack length is increased, the crack will not grow in an unstable way until a certain K, the critical K, is reached. This critical K is denoted by K_c. The crack will start to grow unstable if K is larger than K_c.

Ideally, the critical stress intensity factor, K_c, can be used to predict the behaviour in an actual structure. However, K_c depends on test temperature, specimen thickness and constraint. Beyond a certain thickness, when the material is predominantly in plane strain and under maximum constraint (mode I) the value of K_c tends to a constant lower limit, K_{Ic}, the plane strain fracture toughness. K_{Ic} may be considered a material property. The K_{Ic} indicates whether the material fails ductile or brittle, the higher the K_{Ic}, the more ductile the material. The American Society for Testing Materials (ASTM) published a standard for plane strain K_{Ic} testing, ASTM E399 [23]. The property K_{Ic} determined by this test method characterises the resistance of a material to fracture in a neutral environment in the presence of a sharp crack under severe tensile constraint.
A more detailed description of the ASTM E399 standard will be given in the following section.

2.3.1 The ASTM E399 standard [23]

The ASTM E399 standard provides regulations to obtain plane strain fracture toughness values of metallic materials.
To measure K_{Ic} values of materials, a few standard specimen geometries are designed. In figure 2.6 [23] the available standard specimen geometries: the bend, the compact tension, the arc-shaped tension, the disk-shaped compact tension and the arc-shaped bend specimen are shown.

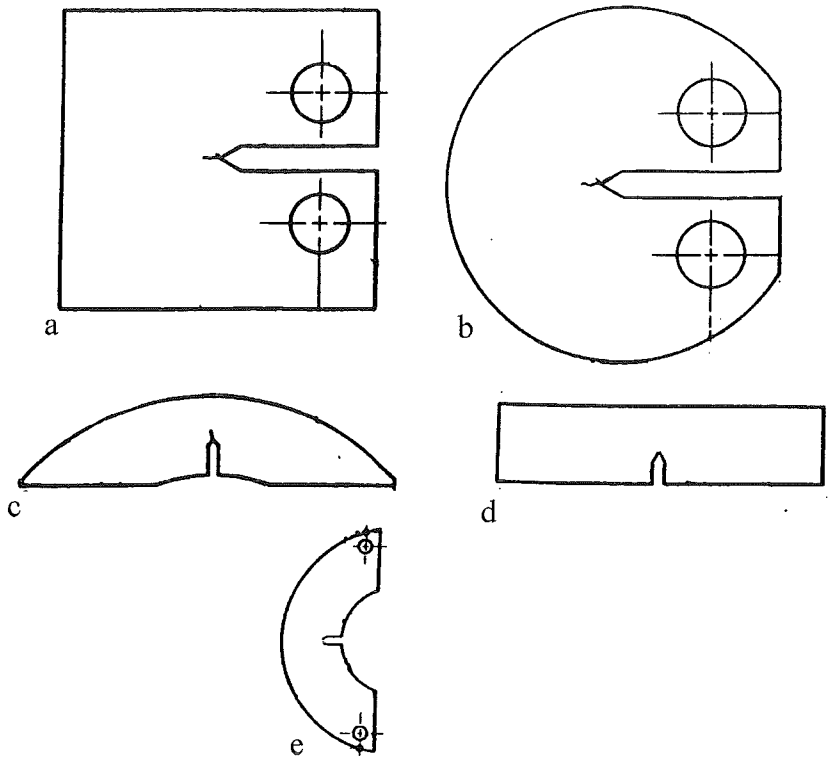

Figure 2.6: (a) compact tension specimen (b) disk-shaped compact tension specimen (c) arc-shaped bend specimen (d) bend specimen (e) arc-shaped tension specimen [23]

For all of these specimen configurations strict size regulations have to be met to ensure plane strain conditions at the crack tip. Furthermore, it is recommended that at least three replicate tests are made for each material condition.
Since the mmc material is an extruded rod with diameter 50.8 mm, the disk-shaped compact tension specimen will be used. The AA6061 material is delivered in a rod of 63.5 mm diameter.
In the stress intensity analysis, see equation 2.3, it is assumed that the crack tip radius is zero. For this analysis to be valid, an ideal plane crack with essentially zero tip radius needs to be simulated. The standard way to obtain such a crack is to fatigue load a specimen until a crack of the desired length has grown. Fatigue loading is done by cyclically loading the notched specimen with a ratio of minimum to maximum stress, R, between -1 and + 0.1 for a number of cycles usually between about 10^4 to 10^6. The number of cycles depends on specimen size, notch preparation and stress intensity. It should be noted that the maximum stress intensity in the final stage of fatigue crack growth is not allowed to exceed 60% of the K_{Ic} value of the material.
The total crack length of the crack starter configuration and the fatigue crack has to be between 0.45 and 0.55 times the width, W, of the specimen. Fatigue precracking must be conducted in the same condition the K_{Ic} test is done. So, the specimens were heat treated before fatigue precracking.

When the specimens are precracked, the actual K_{Ic} test can be performed. The specimens are loaded until fracture, while load and displacement are recorded. From the load-displacement record P_{max} and P_Q are determined. In figure 2.7 three examples of load-displacement records are shown.

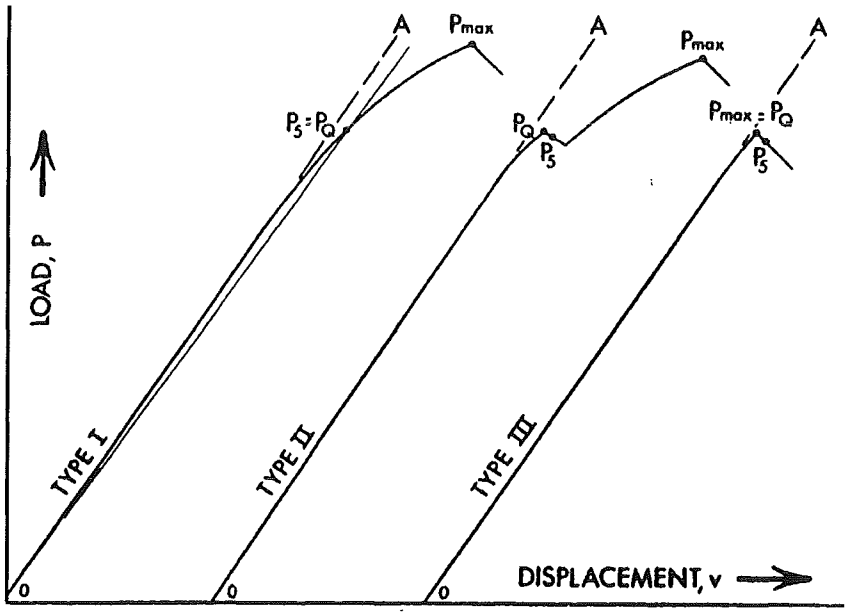

Figure 2.7: The determination of P_Q and P_{max} from three types of load-displacement records [23]

To determine P_Q, a secant line with a slope 95% of that of the linear part of the load-displacement record is drawn. This 95% secant corresponds with a crack growth of 2% of the begin crack length. This 2% crack growth accounts more or less for the effects of plasticity and stable crack growth [23]. The point at which this secant line crosses the load-displacement record is called P_5. If the load at every point that precedes P_5 is lower, than P_Q is equal to P_5. If P_5 is preceded by a maximum than that maximum is P_Q. If the dimensions of the specimen are measured and the geometry factor is known, K_Q can be calculated using equation 2.4.

$$K_Q = \frac{P_Q}{BW^{\frac{1}{2}}} f\left(\frac{a}{W}\right) \tag{2.4}$$

where: P_Q is the load determined from the load-displacement record
B is the specimen thickness
W is the specimen width
$f\left(\frac{a}{W}\right)$ is a geometry factor that differs for the various specimen geometries

For the disk-shaped compact tension specimen used, the geometry factor is given by equation 2.5:

$$f\left(\frac{a}{W}\right) = \frac{\left(2+\frac{a}{W}\right)\cdot\left(0.76+4.8\frac{a}{W}-11.58\left(\frac{a}{W}\right)^2+11.43\left(\frac{a}{W}\right)^3-4.08\left(\frac{a}{W}\right)^4\right)}{\left(1-\frac{a}{W}\right)^{\frac{3}{2}}} \tag{2.5}$$

where: a is the crack length
W is the specimen width

For the K_Q value to be a valid K_{Ic} value according to this testing method, several requirements must be satisfied:

1. For all specimen configurations, the specimen thickness, B and the crack length, a should exceed $2.5(K_Q/\sigma_{ys})^2$, where σ_{ys} is the 0.2% offset yield strength of the material for the temperature and loading rate of the test.

2. The ratio of P_{max}/P_Q is not allowed to exceed 1.10.

3. The crack length, a, after fracture has to be measured at the following three positions: at the centre of the crack front, and midway between the centre of the crack front, and the end of the crack front on each surface of the specimen. The average of these three measurements is used to calculate K_Q.
   The requirements for the fatigue crack front are:
   (a) The difference between the average and the measured crack length at the points should not exceed 10%.
   (b) For a chevron notch starter, the fatigue crack shall emerge from the chevron on both surfaces of the specimen, neither surface crack length shall differ from the average length by more than 10%, and the difference between these two surface measurements shall not exceed 10% of the average crack length.
   (c) For a straight-through starter notch no part of the crack front shall be closer to the machined starter notch than 2.5% W or 1.3 mm, nor shall the surface crack length measurements differ from the average crack length by more than 15%, and the differences between these two measurements shall not exceed 10% of the average crack length.

4. For a valid K_{Ic} measurement the crack plane has to be parallel to both the specimen width and thickness direction within 10°.

If and only if all these requirements are met, the calculated K_Q value is a valid K_{Ic} of the material.

2.3.2 Reported K_{Ic} Values of AA6061 and AA6061 Based MMCs

The reported K_{Ic} values for AA6061 in T6 condition range from 26.6 to 37.0 MPa$\sqrt{m}$. The reported K_{Ic} values for AA6061 reinforced with particles range from 11.1 MPa$\sqrt{m}$ for AA6061 reinforced with 25 vol.% SiC particles to 24.2 MPa$\sqrt{m}$ for AA6061 reinforced with 10 vol.% Al_2O_3 [2]. In figure 2.8 K_{Ic} values found in literature are presented versus volume fraction of the reinforcement. The tougher AA6061 metal matrix composites, approach the lower values reported for the unreinforced alloy [2]. In general it is thought that the toughness of particle reinforced aluminium is very poor, but considering the brittleness of the reinforcing particles, the toughness of AA6061 mmcs is reasonable. The lower fracture toughness in metal matrix composites is partly due to low strain to failure of the reinforcement [2].
The principal cause for the still reasonable toughness of metal matrix composites is that they are essentially metallic. Metallic materials have a process zone that is ductile, and a wide plastic zone around the crack tip. AA6061 metal matrix composites also have a relatively ductile process zone and a reasonably wide plastic zone around the crack tip.

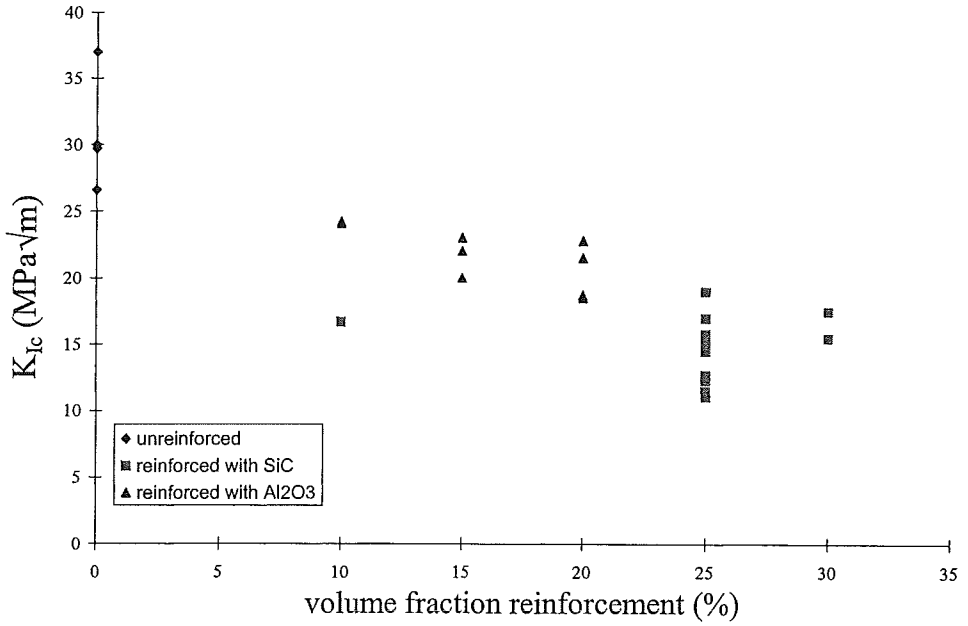

Figure 2.8: K_{Ic} values for AA6061 unreinforced, reinforced with alumina and reinforced with SiC [11]

According to Mortensen [3] it is not possible to detect a difference in K_{Ic} values between Al_2O_3 and SiC particle reinforcement. However, in figure 2.8 it seems that the K_{Ic} of AA6061 reinforced with alumina tends to be higher than that of Al6061 reinforced with SiC.
Hadianfard et al. [7, 10] concluded that Duralcan composites are significantly tougher than Comral composites. Duralcan material is produced by the Alcan Aluminium Corporation and Comral material is produced by the Comalco Research Centre in Melbourne. This lower toughness is probably due to the higher silicon, iron, chromium and titanium contents in Comral-85. These elements form precipitates during heat treatment. These precipitates can form voids during fracture, see section 2.4.2.

2.4 Failure Mechanisms in AA6061

Macroscopically, fracture of most aluminium alloys is tough. The ultimate strain of AA6061 is about 13% in T6 condition [24].
Microscopically, the process of fracture consists of void nucleation followed by void growth and coalescence. In the present aluminium alloy, voids can nucleate on precipitates by decohesion of the interface between precipitate and matrix, or by rupture of the precipitate.
In figure 2.9 the process of void nucleation in the presence of precipitates and subsequent void growth is shown.

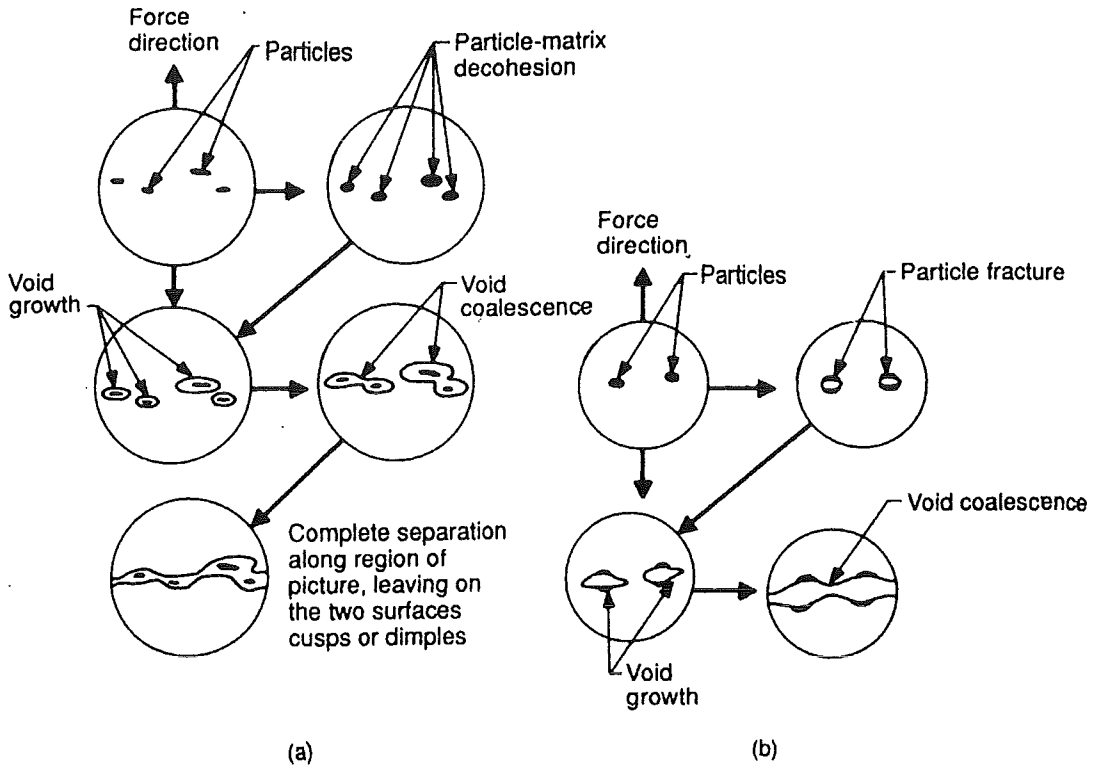

Figure 2.9: Schematic illustration of void nucleation at particles (a) Initiation by particle/matrix interface decohesion (b) Initiation by particle fracture [25]

2.4.1 Interaction Between Cracks and Particles in MMCs

Considering AA6061 particle reinforced composites, they can fracture brittle at a macroscopic scale with an ultimate strain of 4% when containing 20 vol.% of Al_2O_3 particles [24]. Microscopically seen, the matrix fails by void growth and coalescence, as does the AA6061 material without reinforcing particles.
Although the failure mechanisms are microscopically the same, the presence of brittle particles in a ductile matrix can have effects on the actual failure mechanism.

There are several ways of interaction between a growing crack and the reinforcing particles in a particle reinforced composite. First, cracked particles can initiate a crack through the matrix. These particles then act as nucleation sites for voids. These voids will grow and subsequently be linked to each other, which causes macroscopic failure. It might be possible that the crack path followed, is the one that contains the most broken particles. If this mechanism is responsible for failure, a relatively large percentage of broken particles should be seen at the fracture surfaces [2].

Another possible mechanism of fracture in composites is that of particle/matrix debonding or decohesion, followed by matrix failure. If this mechanism occurs, few or no broken particles should be seen at the fracture surfaces. Wei and Huang [26] proposed that debonding is a crack blunting mechanism and that it would be beneficial for the toughness of the mmc if debonding occurs.

Mummery and Derby [27] proposed a simple stress criterion whereby fracture nucleates when the local stress exceeds either the interfacial bond strength or the fracture strength of a particle. If the interfacial bond strength is exceeded, decohesion will occur. If the fracture strength of the particle is exceeded, particle cracking will occur.

A third failure mechanism can be found when microcracks, formed in front of the crack, are linked to the crack by void growth. As the result of inhomogeneous deformation, high local stresses can arise in front of the crack mouth leading to microcracks. Microcracks can exist in particles as well as in the matrix [28].

2.4.2 Influence of Heat Treatment on the Fracture Mechanisms of MMCs

Ageing changes the matrix microstructure and can therefore change the fracture mechanism.
Hadianfard et al. [7, 10] have investigated the fracture surface of underaged (0.75 hr/ 175°C), peak aged (8 hr/ 175 °C) and overaged (24 hr/ 175 °C) AA6061 reinforced with 20 vol.% Al_2O_3.
The fracture morphology of the underaged specimens was characterised primarily by large deep voids centred on large fractured particles with secondary void nucleation and growth in the matrix. Two different populations of voids were found, one with an average size of 21 μm and one with an average size of 7.6 μm. About 17.6% of the fracture surface was covered by broken alumina particles. The primary voids were nucleated at low strain by particle cracking. The matrix showed shear and, what Hadianfard et al. call, shear lips between particles.
The fracture surfaces of the overaged specimens were covered with large and small shallow voids. The large voids were formed around the large alumina particles by separation of the matrix/particle interface. Three different populations of voids could be seen, one with an average size of 17.5 μm, one with an average size of 6 μm and one with an average size of 2.6 μm. In the overaged condition only 8% of the fracture surface was covered with fractured alumina particles. The presence of precipitates near the matrix/particle interface reduced the surface energy of the interface or decreased the bond strength of the matrix and the Al_2O_3 particles. This constituted an easy path for crack growth.
On the fracture surface of the peak aged specimens a large number of microvoids with different sizes were observed. These microvoids were formed in the matrix/particle interface, close to large alumina particles and in the matrix, similar to the voiding observed in the overaged condition.

The larger voids in the underaged, overaged and peak aged condition were due to debonding of the matrix/particle interface or particle cracking. The small voids in the overaged and peak aged condition were due to precipitates that acted also as void nucleation sites. More void nucleation sites led to more voids and therefore to less void growth before the voids coalesced. This reduced the fracture toughness of the material.

Klimowicz and Vecchio [29] found similar features in AA6061 reinforced with 15 vol.% Al_2O_3 particles. The primary dimples in the underaged (1 and 3 hrs/ 177°C) samples were very deep and their walls were covered with fine lines, as a result of serpentine glide indicating ductile failure of the matrix. The overaged samples (25 and 100 hrs/ 177°C) showed smaller dimples and no signs of serpentine glide.

Shyong and Ruiz [30] investigated the fracture surfaces of AA6061 reinforced with 5, 10 and 20 vol.% SiC particles. In the naturally aged condition the dimples on the fracture surface were shallower than in the overaged condition. The fracture surface of a particle showed a river pattern, indicating a brittle fracture.

Dutta and Majumbar [31] concluded that in the T6 condition, crack propagation was controlled by particle fracture, whereas after sub-solvus anneal (i.e. 8 hrs at 450°C), fracture was controlled by matrix failure. This was concluded for AA6092 (nearly identical to AA6061 only a slightly higher Cu content) reinforced with 17.5 vol.% SiC particles. In the T6 condition an abundance of fractured particles could be seen on the fracture surface. The matrix was, in this condition, strong enough to load the particles to their fracture stress.
In the sub-solvus annealed condition only a few particles were seen within the dimples. The particles were not loaded to their fracture stress since matrix failure occurred first. This resulted in matrix-controlled crack initiation and propagation, and a high corresponding fracture toughness.

2.5 The Model of Hahn and Rosenfield [5]

A model proposed by Hahn and Rosenfield, can be used to discuss the effect of second phase particles in ductile fracture. According to Rabiei et al. [5] this model might be suitable for mmcs to predict the K_{Ic}.
The Hahn and Rosenfield model, assumes uniformly distributed spherical particles with a certain diameter. A present crack starts to grow when the crack tip opening displacement, δ, becomes equal to the average spacing between the particles.

The average spacing λ between the particles is given by:

$$\lambda = \left(\frac{\pi}{6}\right)^{\frac{1}{3}} D V_f^{-\frac{1}{3}} \tag{2.6}$$

The critical crack tip opening displacement δ_c is given by:

$$\delta_c = \frac{K_{Ic}^2}{2\sigma_y E} \tag{2.7}$$

Combining equations (2.6) and (2.7) with $\delta_c = \lambda$ results in:

$$K_{Ic} = \left[2\sigma_y E\left(\frac{\pi}{6}\right)^{\frac{1}{3}} D\right]^{\frac{1}{2}} V_f^{-\frac{1}{6}} \tag{2.8}$$

where: σ_y is the yield strength of the composite or matrix
E is the Young's modulus of the composite
D is the particle diameter
V_f is the volume fraction of particles in the composite

Using equation (2.8) K_{Ic} values can be predicted. There is some confusion as to whether the composite or matrix yield stress should be used in this equation. When the plastic zone is large, the size of the zone is affected by the properties of the composite and the yield stress of the composite should be used. When the plastic zone is small, few reinforcing particles are within the plastic zone and the yield stress of the matrix is probably more appropriate [1].

To verify the assumption that the crack will grow when the crack tip opening displacement is equal to the spacing between particles, λ en δ_c can be calculated after K_{Ic} is calculated.

3. EXPERIMENTAL PROCEDURES

3.1 Materials Used

The AA6061 aluminium alloy was produced by Cressona Aluminum Company, the Unites States. The material was extruded to a diameter of 63.5 mm and delivered in T651 condition.
The chemical composition limits of AA6061 alloys are given in table 3.1. The values for Fe, Mn, Ti and Zn are maxima.

Table 3.1 : The chemical composition limits of AA6061 in weight percentage.

Si	Mg	Fe	Cu	Cr	Mn	Ti	Zn	Al
0.4-0.8	0.8-1.2	0.7	0.15-0.40	0.04-0.35	0.15	0.15	0.25	Rest

The metal matrix composite used was produced by Duralcan USA, which is a division of Alcan Aluminum Corporation. The mmc was produced via the stir casting process. In stir casting, the reinforcing powder is added and mixed into the molten matrix through melt agitation by a stirrer. After stir casting, conventional metal processing techniques can be used. In this case, the material was extruded into a rod with 2-inch diameter.
As the matrix is AA6061, it should meet the chemical composition limits given in table 3.1.

The exact chemical compositions of the mmc and the AA6061 alloy can be determined with X-ray fluorescence. The samples for X-ray fluorescence should not be ground because during grinding silicon particles can be rubbed in the material, thus leading to an overestimation of the silicon content.

3.2 Heat Treatment

Two hot air furnaces were used for heat treatment of the specimens. One, a circulation hot-air furnace made by Degussa, was kept at 530 °C for solutionizing. The other also a circulation hot-air furnace made by Snijstaal Fabricage B.V. was used for subsequently heating the specimens at a rate of 5 °C/min until the temperature at the end of peak B or C was reached, see figure 2.1.
To investigate the response of the Snijstaal furnace and the specimens to the heating rate, a few test runs were performed. One specimen was used as dummy, in which a hole was drilled to insert a nickel chromium/nickel aluminium thermocouple (type KX). The thermocouple registered the temperature at the centre of the dummy.
To verify the calibration of the thermocouple, the temperatures of ice and boiling water were measured. The thermocouple registered these temperatures with acceptable accuracy.
A x-y plotter (Kipp & Zonen BD41) was attached to the thermocouple to register the heating rate in the centre of the dummy specimen, see appendix 1.
During heating, the heating response of the specimens was retarded because the heat had to be transferred from the furnace to the specimens. Since the thermal conduction of aluminium is good, the temperature will be nearly uniform throughout the specimen.

This means that the heat resistance of the specimen surface determined the difference in temperature between specimen and furnace.
The runs were reproducible. The temperature difference was nearly constant and depended on the specimen geometry and the specimen material. So, for every specimen geometry and specimen material a dummy sample is needed.
Two different programs were written for the Snijstaal furnace. One to obtain the temperature after peak B (256 °C for the base material 254 °C for the mmc) and one to obtain the temperature after peak C (309 °C for the base material 300 °C for the mmc). DSC studies of AA6061 have indicated that there was only one small peak beneath 100°C associated with Mg, Si or vacancy clustering. After this small or sometimes non-existing peak, nothing happened until 200°C was reached. Because it was difficult to heat the specimens from ambient temperature to 300 °C with a constant rate of 5 °C/min, a two step heating program was chosen. The specimens were heated either to 80 °C for the specimens heated till after peak B or to 100 °C for the specimens heated till after peak C. The specimens were kept at that temperature for 20 minutes so that the specimen temperature was uniform throughout the whole specimen. After that, the specimens were heated with a rate of 5 °C/min until the desired temperature was reached and were immediately water quenched. The heat treatments following the solution heat treatment are schematically shown in table 3.2.

Table 3.2: Scheme of the heat treatments for AA6061 and mmc in B and C condition

material	step 1 temperature (°C)	Time at step 1 temperature (minutes)	temperature to reach (°C)	Time to reach temperature(minutes)
AA6061 B	80	20	256	35
AA6061 C	100	20	309	42
Dur B	80	20	254	35
Dur C	100	20	300	40

From this point forward, the heat treatments described will be referred to as heat treatments B and C.

3.3 Tensile Tests

The K_{Ic} tests were performed on specimens whereby loading was perpendicular to the extrusion direction. Therefore, tensile specimens were taken from the extruded bar the same way. The specimen geometry used is a proportional reduced pin-loaded tension test specimen described in the ASTM standard E8M [32]. The specimen geometry is shown in figure 3.1.

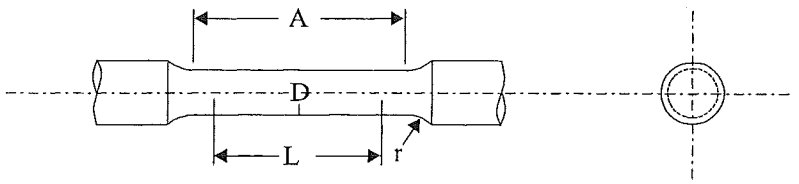

Figure 3.1: The specimen geometry used for the tensile tests, where L= mm, A= mm, r=3 mm, and D = 6 mm.

The specimens were provided with threaded ends to connect them to extension pieces. These extension pieces were fixed in the wedge grips of the tensile test machine. The extension pieces were assumed to be infinitely stiff, since they were made of steel and will not deform under the used maximum load of approximately 10 kN.
Because the different heat treatments led to different precipitate structures in the matrix, the mechanical properties will differ in these different heat treatment conditions.
Two tensile tests were performed in each condition: the as-received T651 condition, and the conditions after heat treatments B and C, see section 3.2.
For all tests, an Instron 4505 testing machine with a 100 kN loadcell was used, see appendix 2. This tensile testing machine was fitted with a stress-strain function panel. The data was recorded by a computer using 'Series IX Automated Materials Testing System 5.04' software. The tensile tests were performed computer controlled and under displacement control. During displacement controlled loading the lower traverse moved down with a fixed rate (the rate used was 0.5 mm/min).
In order to measure the displacement, an Instron clip gauge of 12.5mm ± 5mm was used, see figure 3.2.

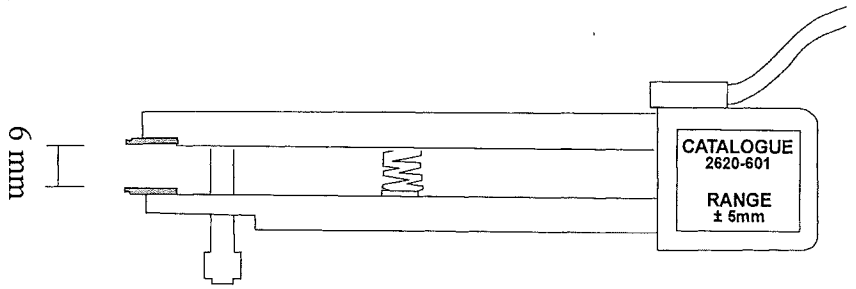

Figure 3.2: The clip gauge used for tensile and K_{Ic} testing

The gauge length was increased to 25 mm with standard extension pieces and the clip gauge was fixed to the specimen with rubber bands.

To prevent damage of the clip gauge, it had to be removed before specimen fracture. A change from clip gauge displacement to cross head displacement could be programmed in the test. The computer gave a warning signal when changing the data acquisition from clip gauge to cross head displacement after which the clip gauge could be removed without stopping the test. In the output data the change in acquisition was not visible.

3.4 K_{Ic} tests

3.4.1 Specimen Geometry

The specimen geometry used was the disk-shaped compact tension specimen. The measures of the specimen can be seen in figure 3.3.

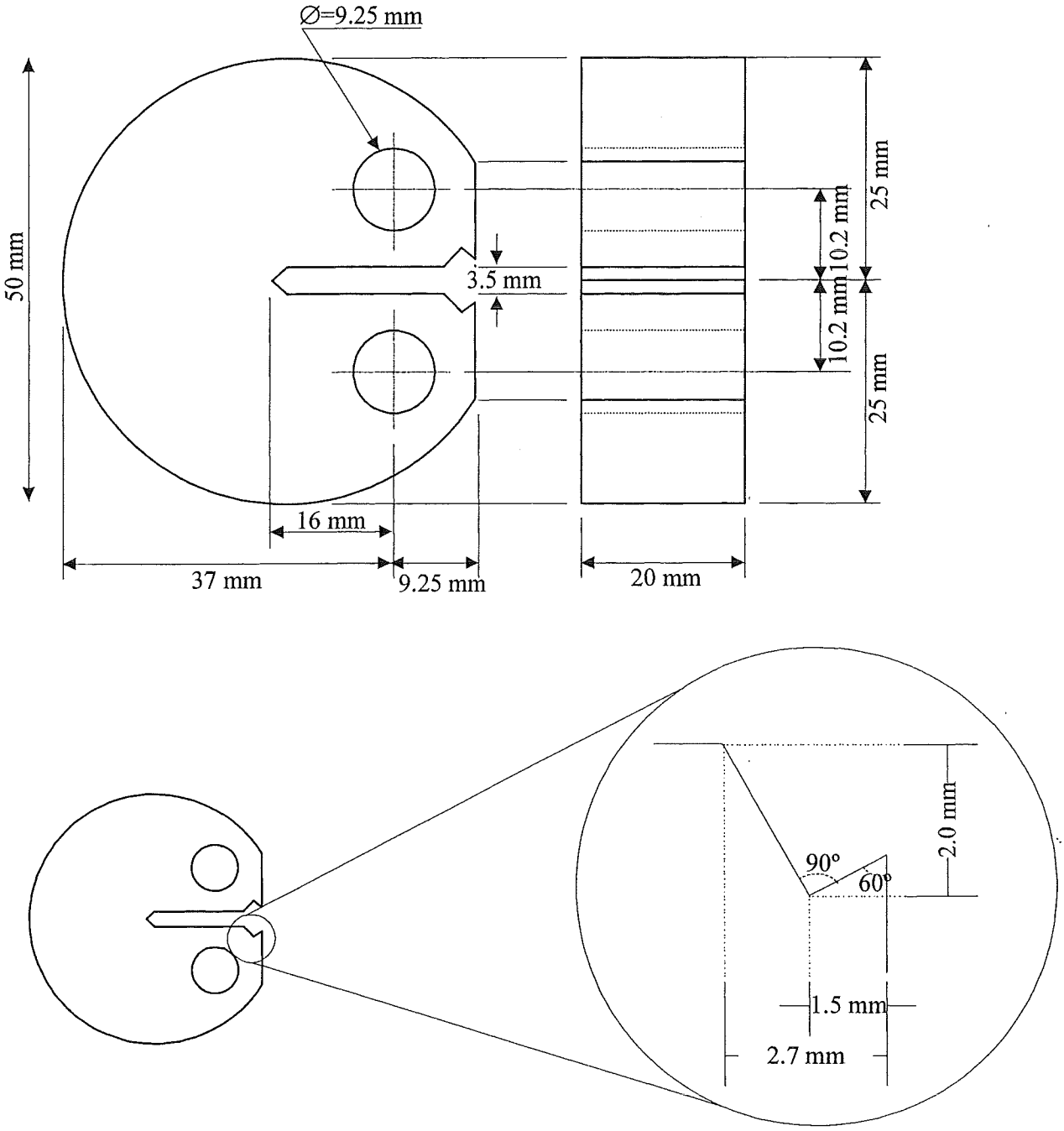

Figure 3.3: The dimensions of the K_{Ic} specimen used

The available materials were extruded rods. To make the specimens, disks of 19.4 mm thick were sawn from the rods. These disks were machined to exactly 50 mm diameter.

The specimens were cut from the disks using the high-pressure waterjetting technique. With this technique, the specimens were cut with a high-pressure water jet with abrasives. The water pressure used was 3800 bar and the diameter of the jet before adding the abrasive was 0.3 mm. The abrasive was HP-Barton Granat mesh#150. It consisted mainly of SiO_2, Al_2O_3 and Fe_2O_3. At the end of the nozzle the abrasive was added, the diameter of the jet was then 0.8 mm and that was also the diameter of the jet when reaching the specimen. The amount of water and abrasive per minute was respectively 2 - 2.5 l/min and 250 g/min.
A disadvantage of this technique is, that the water jet fans out through the thickness of the material, which leads to broadening of the notch on one of the sides.

3.4.2 Fatigue Precracking (Dynamical Part of the Test)

The fact that the notch of the specimen after waterjetting was a bit sharper on one side of the specimen and more blunt on the other, led to problems with fatigue precracking. Initiation of the fatigue precrack occurred first on the side with the sharper notch. Furthermore, the fatigue precrack did not straighten during crack growth. To produce valid K_{Ic} values the fatigue precrack was not allowed to be too oblique.
During the fatigue precracking, the crack can also tunnel. This tunnelling meant that the crack grew harder in the centre than at the surfaces. A parabolic crackfront was obtained if a fatigue crack tunnelled.
If the crackfront was straight the stress state in the centre of the specimen during the actual K_{Ic} test was plane-strain like, meaning that the specimen did not strain in the direction perpendicular to the loading direction. In the case of a tunnelled crack the material was able to strain perpendicular to the applied stress, the stress state became more or less plane stress.

Every crackfront is to a certain degree oblique and tunnelled. To determine the amount of obliqueness and tunnelling the following equations were used.

The amount of obliqueness is given by:

$$\left(\frac{a_{surf,max} - a_{surf,min}}{a_{surf,min}} \right) \tag{3.1}$$

The amount of tunnelling is given by:

$$\left(\frac{a_{max} - a_{obl,x}}{a_{obl,x}} \right) \tag{3.2a}$$

$$a_{obl,x} = a_{surf,max} - \left(x \cdot \frac{a_{surf,max} - a_{surf,min}}{B} \right) \tag{3.2b}$$

where: a_{max} is the maximum of a
$a_{surf,max}$ is the maximum of a at the surface
$a_{surf,min}$ is the minimum of a at the surface
B is the specimen width
x is the position of the maximum crack length

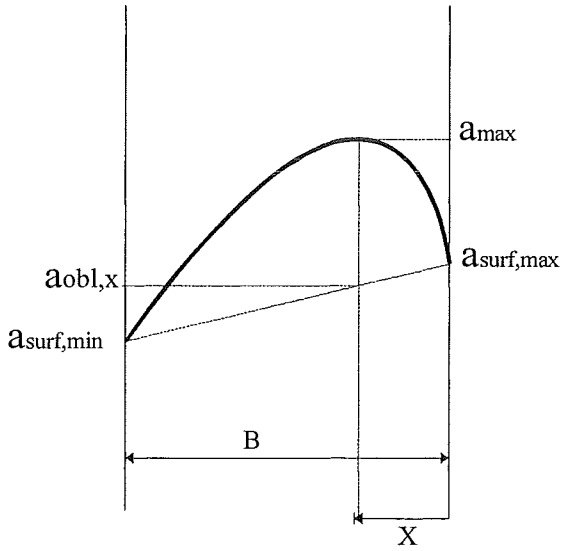

Figure 3.4: A crack front with the crack length measurements necessary to calculate the amount of obliqueness and tunnelling

If after high-pressure waterjetting, the notch was spark-machined, a straight sharp notch could be formed. It was thought that if the notch then was sharp enough, it might be possible to omit precracking. To investigate whether the spark-machined notch was sharp enough to yield reasonable and valid K_{Ic} values, three specimens were made this way and tested. It turned out that because of the compactness and the thickness of the specimens there was still a large chance that the fatigue precrack, even after spark-machining, would become oblique.
The specimens gave K_Q values that were much too high, so the specimens do indeed require fatigue precracking after spark-machining.

As can be seen in chapter 4, the crack fronts of the AA6061 specimens were oblique and/or tunnelled. There was reason to believe that crack tunnelling would become an even bigger problem in the composite materials, because of residual stresses [11]. These residual stresses occur during cooling because of the difference in thermal coefficient between matrix and reinforcement material.
The problem of oblique fatigue precracking can usually be overcome by changing the straight through notch into a chevron notch. The composite specimens should therefore have chevron notches.

It is practically impossible to produce a chevron notch by high-pressure waterjetting, because the waterjet should then enter at an angle. However, the position of the waterjet is fixed. The chevron notch could be made with spark-machining. A copper sheet was used instead of the more frequently used copper wire and the specimen was fixed in such a way that the top angle of the notch was 120°.
To prevent crack tunnelling, the applied load used during fatigue precracking was kept low after crack initiation. With a TL light and loupe it was easy to detect the fatigue crack in AA6061 during fatigue loading before the upper limit of the crack (a = 0.55W) was reached.
In the composite material however, the crack turned out to be invisible during fatigue precracking. Twice the crack was not detected in time resulting in broken specimens during fatigue precracking. In other specimens, a crack seemed to appear but was, as could be seen after K_{Ic} testing, not there at all. Even after grinding and polishing the specimens up to 0.25 μm the crack could not be detected on the outside.

With a clip gauge it was possible to measure the crack mouth opening displacement (CMOD) of a specimen during fatigue precracking. If a crack grows, the compliance of the specimen will enhance and the CMOD becomes larger under the same applied load. Every certain number of cycles, the CMOD was measured at P_{max} and P_{min}, see equations 3.3a and b. The compliance of the specimen after those cycles is given by equation 3.3c.

$$\Delta CMOD = CMOD_{P_{max}} - CMOD_{P_{min}} \tag{3.3a}$$

$$\Delta P = P_{max} - P_{min} \tag{3.3b}$$

$$C = \frac{\Delta CMOD}{\Delta P} \tag{3.3c}$$

where: C is the compliance
P_{max} is the maximum load during a fatigue cycle
P_{min} is the minimum load during a fatigue cycle
CMOD is the crack mouth opening displacement

Jablonski et al. [33] have fitted compliance functions for various fracture toughness specimens. For the disk-shaped compact tension specimen the fitted equation was:

$$\ln\left[\frac{E' V_x B}{P}\right] = \sum_{i=0}^{5} A_i \left(\frac{a}{W}\right)^i \tag{3.4}$$

where: B is the specimen thickness
E' is the plain strain Young's modulus
P is the applied load
V_x is the crack opening displacement at location x from the load line
A_i are coefficients as listed in table 3.3
a is the crack length
W is the specimen width

The plain strain Young's modulus is given by equation 3.5:

$$E' = \frac{E}{1-\nu^2} \tag{3.5}$$

where: E is the elastic modulus
ν is Poisson's ratio

Table 3.3: The values of the coefficients A_i in equation 3.4 for a disk-shaped compact tension specimen [33]

Location	A_0	A_1	A_2	A_3	A_4	A_5
front face	2.456	-0.483	13.996	-18.708	8.493	3.571
load line	0.973	6.573	-8.117	21.532	-29.248	17.488

When measuring the crack mouth opening displacement at the front face, (the CMOD equals V_x), equation 3.4 can be simplified in:

$$\ln[E' CB] = \sum_{i=0}^{5} A_i \left(\frac{a}{W}\right)^i \tag{3.6}$$

Equation 3.6 links the compliance calculated with equation 3.4 to the crack length in the specimen.
With this method the crack length could be calculated and it was not necessary to detect it visually. Equation 3.6 was used to calculate the crack length at any given compliance, with the computer program Maple, version 4.
A polynome was fitted through the points, so that if the compliance was measured during precracking the crack length could be calculated directly with equation 3.7.

$$a = -0.0063C^2 + 0.632C + 5.4419 \tag{3.7}$$

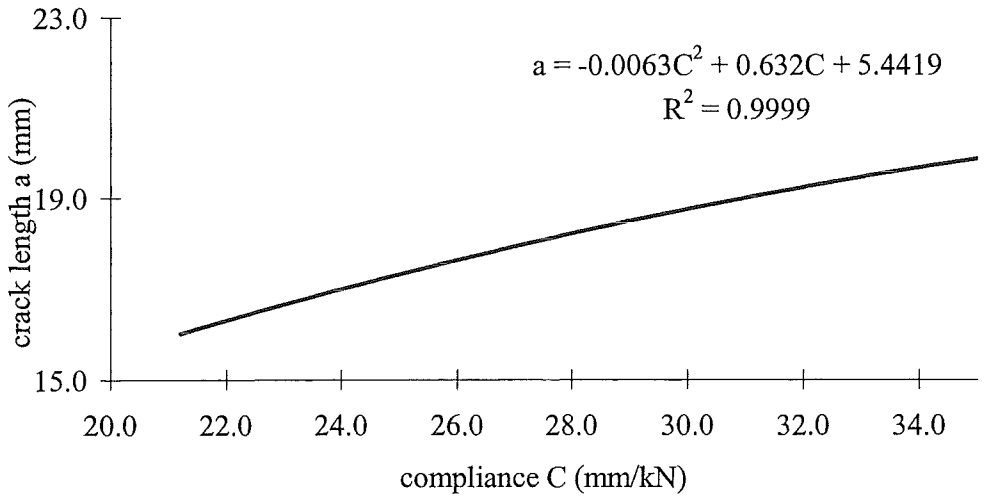

Figure 3.5: Crack length a as a function of compliance C

The method did not seem to work accurately during fatigue loading of the first Duralcan specimen, since the compliance did not enhance. This turned out to be a consequence of crack closure. To verify whether crack closure happened during fatigue loading, the load was enhanced in small steps from P_{min} to P_{max}, measuring the CMOD at each step. As figure 3.6 shows, crack closure occurred when the load was less than 0.4 P_{max}.

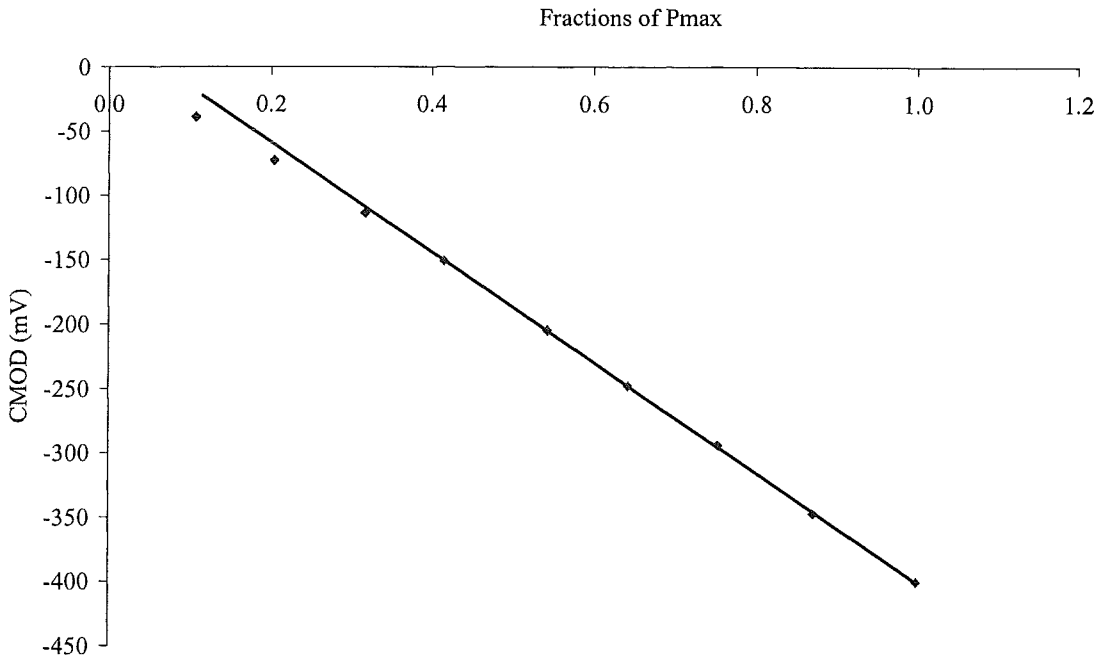

Figure 3.6: CMOD against load indicating crack closure when the applied load is less than $0.4P_{max}$

To overcome this problem of crack closure for the remaining specimens, the load difference was not measured at P_{max} and P_{min} but at P_{max} and 0.5 P_{max}. This changes equations 3.3a and 3.3b as follows:

$$\Delta CMOD = CMOD_{P_{max}} - CMOD_{0.5P_{max}} \quad (3.8a)$$

$$\Delta P = P_{max} - 0.5P_{max} \quad (3.8b)$$

3.4.3 Determination of K_{Ic} (Statical Part of the Test)

When the specimens were fatigue precracked, the actual K_{Ic} test could be done. The specimen was fixed in the grips of the testing machine and the clipgauge, see figure 3.2, was placed in the crack mouth.
To prevent non-linearity at the start of the load displacement diagram, the mmc specimens were loaded to the load level of fatigue precracking, unloaded again and then the test was started. Loading and unloading before the test is done with the same speed as the actual test, 3 mm/min. Loading and unloading to the load level of fatigue precracking can be done more than once.
The increase of the stress intensity factor during the K_{Ic} test was within 0.55 and 2.75 $MPa\sqrt{m}s^{-1}$.

3.4.4 Equipment Used During K_{Ic} Testing

A 25kN Schenck servo-hydraulic fatigue machine was used for fatigue precracking the three AA6061 specimens in received T651 condition. This machine was not operating accurately, so the remaining specimens were fatigue precracked on a 100 kN MTS servo-hydraulic fatigue testing machine. The control unit of the MTS fatigue testing machine was a model 436.11 control unit, this control unit provided centralised manual or automatic control of system electrical power, hydraulic pressure and program wave

form and frequency. Another controller model 406.11, an electronic sub-system containing the principal servo control, failsafe and read-out functions, was also used. The clip gauge used during fatigue precracking was made in the laboratory and connected to a Hellige Mess-und Registriertechnik extensometer type 19. The load and the CMOD were registered with an Olivetti Personal Computer M21. To lower the noise levels of the signals from load and CMOD, an RC-filter was placed between the signal and the computer.
The calibration of the clip gauge was checked before each test using a micrometer.

The actual K_{Ic} tests were performed on an Instron testing machine type 4505 with a 100 kN loadcell. The Instron testing machine can be computer or manual controlled. In manual control different blocks for loading and unloading at a certain speed can be programmed in the control unit. As with the tensile tests, the computer stored the acquired data.
The clip gauge used during K_{Ic} testing was the same as shown in figure 3.2, it was an Instron clip gauge Catalogue 2620-601 with a range of 12.5 mm ± 5 mm.

3.6 Scanning Electron Microscopy

The mmc was difficult to machine, so it was convenient to insert the specimen halves in the Scanning Electron Microscope (SEM) without cutting them into smaller pieces. The fracture surfaces may not be touched and the cleaning should be done with great care. The specimens were first cleaned ultrasonic with acetone to remove all fat and then with propanol to remove all acetone.
The samples were put in a holder and placed in the SEM. The dynamical and statical parts of the fracture surfaces were investigated.
To obtain a clear picture of the AA6061 fracture surfaces, an acceleration voltage of 5 kV was used. For the mmc a clear picture was obtained with an acceleration voltage of 15 kV.

In literature, Mg enrichment around the particles was reported [7, 14, 34, 35] for mmc produced via liquid methods. The Mg forms $MgAl_2O_4$ spinels at the particle/matrix interface when the Al_2O_3 particles are added. The SEM used for the fracture surface investigation is equipped with possibilities to make linescans, pointscans and X-ray maps. In X-ray mapping the amount of an element is measured relative to its surrounding. So when making an X-ray map from a frame the relative amount of O, Si, Mg, Al can be shown. Higher amounts of an element give rise to brighter colours. If there are $MgAl_2O_4$ spinels around the particles, the form of the particles will also be visible in the X-ray map of Mg.
A relatively fast way to detect Mg enrichment in the mmc is to make linescans from the matrix with particles in it. The counts of linescans can not be calculated into atomic percentages, because measurements were made at one point of the Mg peak, in most cases at the top of the peak. So linescans do not give information about the amount of an element relative to the other elements, but it should be able to see the difference between the particles and the matrix in linescans.
The amount of counts from an element can be influenced by height differences. To determine Mg enrichment it is best to use smooth and flat specimens, so they had to be ground and polished.

4. RESULTS OF AA6061

4.1 Chemical Composition of the Material

The chemical composition of the AA6061 material was determined with X-ray fluorescence, and is given in table 4.1.

Table 4.1: The chemical composition of the AA6061 material in weight percentage

Mg	Si	Fe	Cu	Cr	Mn	Ti	Zn	Pb	Ni	Al
0.89	0.63	0.36	0.34	0.10	0.10	0.03	0.023	0.02	0.01	rest

Comparing tables 3.1 and 4.1 shows that the chemical composition of the material is within the composition limits of AA6061. The delivered condition was T651, this heat treatment consists of solutionizing at 530-550°C for 0.5-2 hrs followed by air or water quench. The material is subsequently stretched for 1-3%, then it is artificially aged at 175°C for 8 hrs.
To verify whether different precipitates were formed during the different heat treatments, mentioned in chapter 3, samples were made for X-ray diffraction. The samples needed to be ground and polished to 0.25 μm before measuring them. It proved to be impossible to determine the precipitates in this material. Possible causes for this are, that the precipitates were either too small or that there were not enough precipitates present to detect them.

4.2 Tensile Tests

From the recorded stress-strain curves the Young's modulus (E) the 0.2% yield stress (σ_{ys}), the ultimate tensile strain (ε_{uts}) and the strain hardening exponent (n, using equation 4.1) were determined.

$$\sigma = k \cdot \varepsilon^n \tag{4.1}$$

For σ_{ys} a line parallel to the start of the stress-strain curve is drawn from the point of 0.2% strain and zero stress. The point where this line crosses the stress-strain curve is σ_{ys}.
In table 4.2, the properties determined from the stress-strain curves are given.

Table 4.2: Material properties determined with the tensile tests

specimen	E (GPa)	σ_{ys} (MPa)	ε_{uts} (%)	n
6061-1	77.7	330	11	0.065
6061-2	77.5	299	10	0.079
6061B-1	72.5	338	9	0.086
6061B-2	73.8	318	8	0.083
6061C-1	71.6	232	8	0.130
6061C-2	76.6	232	8	0.130

As can be seen in table 4.2, the measured Young's modulus does not differ so much in the three conditions as do the ultimate tensile strain, the yield stress and the strain hardening exponent.
In C condition the transition of elastic to plastic deformation occurs at lower stress levels then in T651 and B conditions. Considering the yield stress, it can be seen that it is lowest in C condition and the highest in condition B.
For the ultimate tensile strain, B and C condition are equal but both lower than in case of condition T651.
The strain hardening exponent increases going from T651 to B to C condition.
The stress-strain curves are shown in figures 4.1 to 4.6.

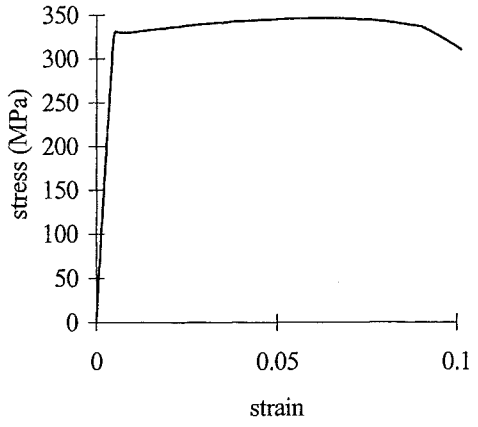

Figure 4.1: Stress-strain curve of 6061-1, AA6061 in T651 condition

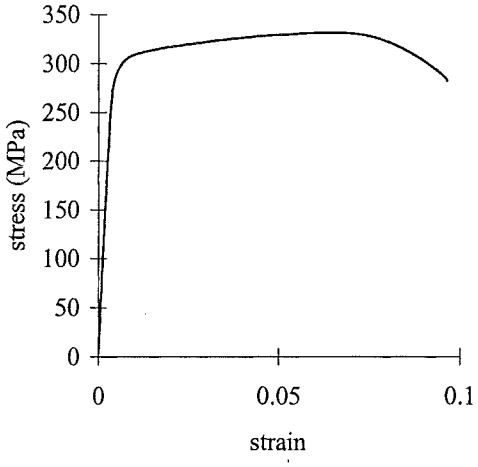

Figure 4.2: Stress-strain curve of 6061-2, AA6061 in T651 condition

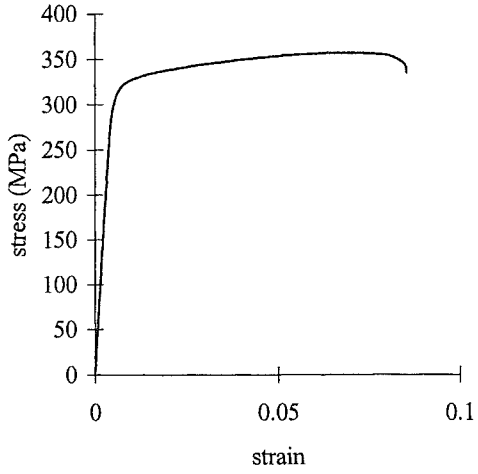

Figure 4.3: Stress-strain curve of 6061B-1, AA6061 in B condition

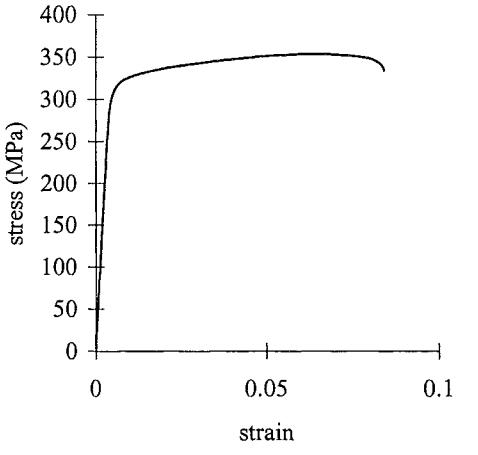

Figure 4.4: Stress-strain curve of 6061B-2, AA6061 in B condition

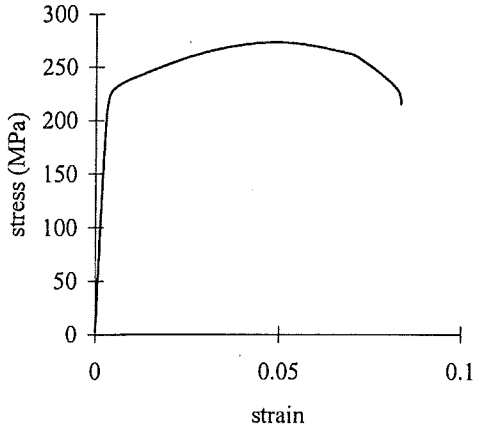

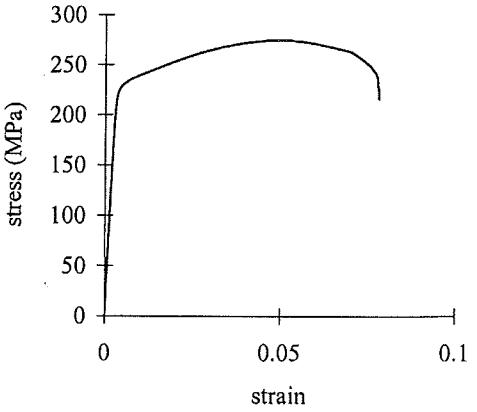

Figure 4.5: Stress-strain curve of 6061C-1, AA6061 in C condition

Figure 4.6: Stress-strain curve of 6061C-2, AA6061 in C condition

In figures 4.7 to 4.9 the fracture surfaces of the tensile specimens in the different heat treatment conditions are shown.

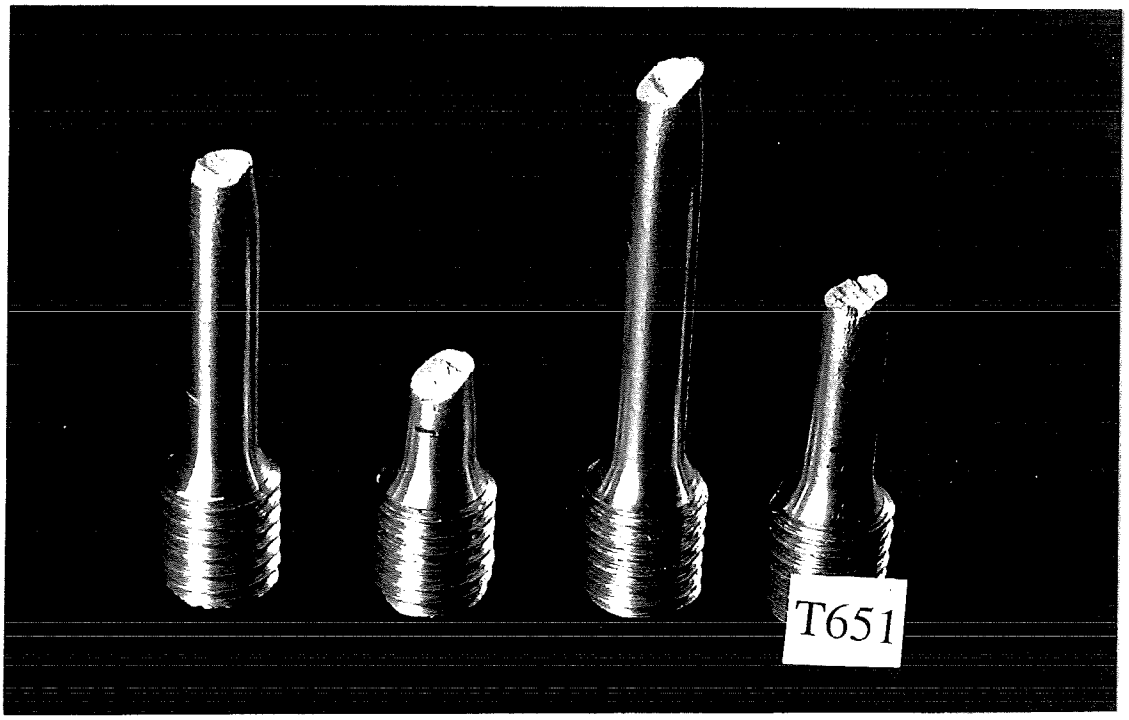

Figure 4.7: Fractured AA6061 tensile specimens in T651 condition

The specimens in figure 4.7 show necking and these fracture surfaces are called cups. The specimens in T651 condition have the largest ultimate strain.

The tensile specimens in B condition show fracture under an angle of 45° to the loading direction, i.e. the maximum shear stress direction. Before fracture occurred scarcely any necking was observed. It should be mentioned that, in contrast to the specimens in T651 and C conditions, the fracture itself produced a bang.

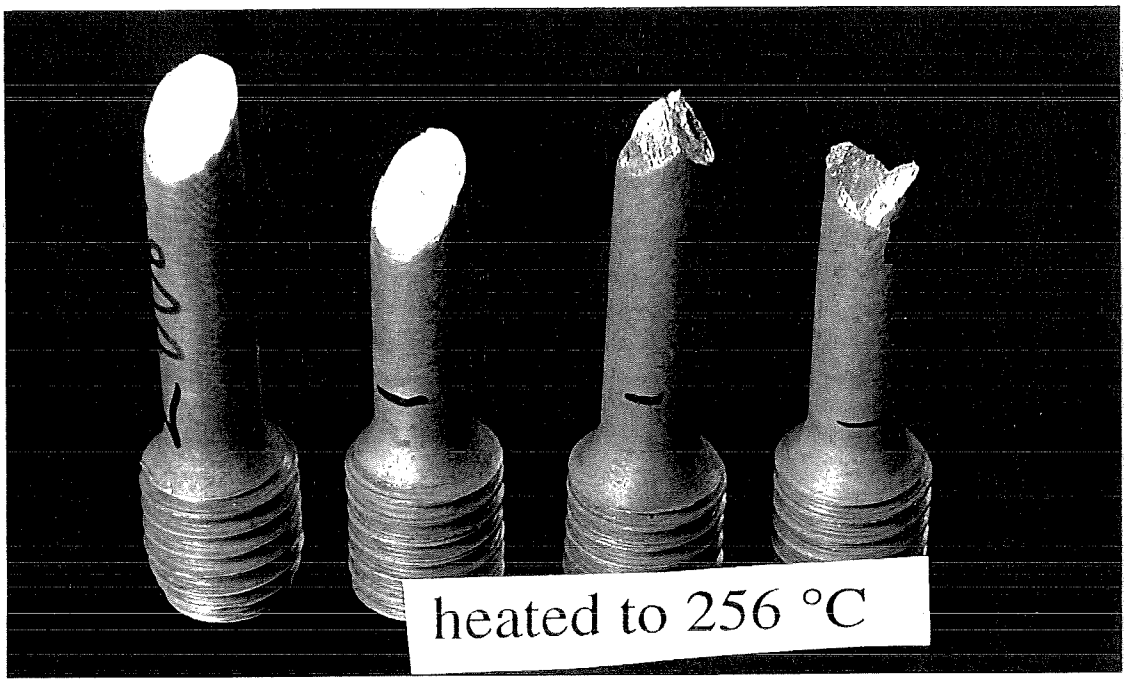

Figure 4.8: Fractured AA6061 tensile specimens in B condition

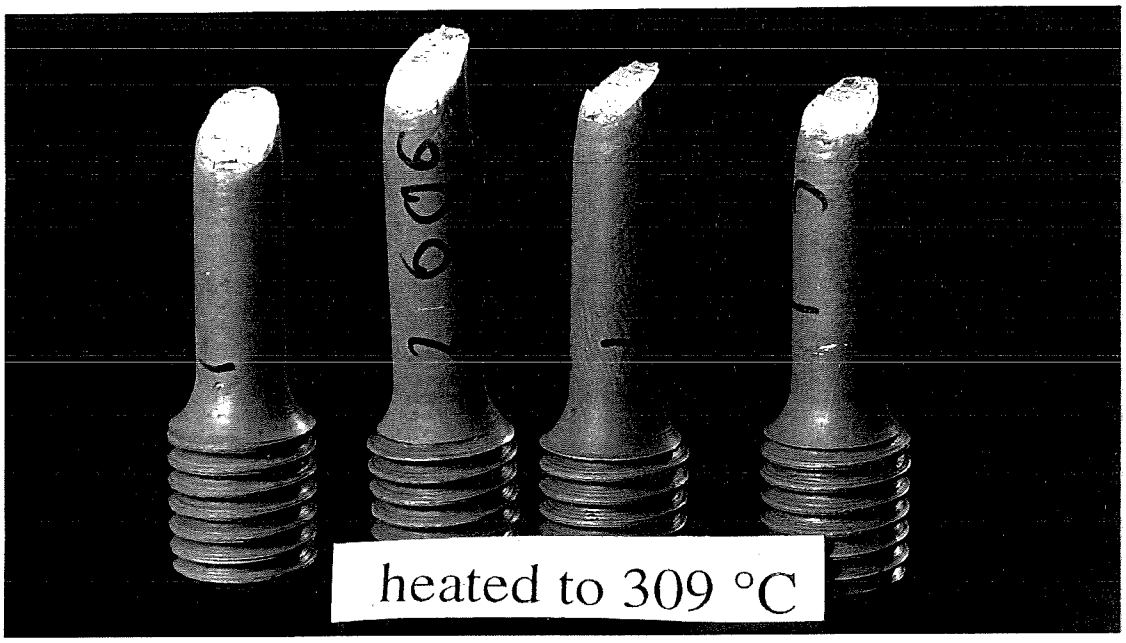

Figure 4.9: Fractured AA6061 tensile specimens in C condition

The tensile specimens in C condition show some necking before fracture, although not to the same extent and more locally then the specimens in T651 condition. The fracture surfaces are also under an angle of 45° to the loading direction.

4.3 K_{Ic} tests

4.3.1 K_Q Values of Specimens with Spark-Machined Notches

In table 4.3, the results of the K_{Ic} tests on specimens with spark-machined notches without precracking can be seen. All values are invalid because the crack length and the

specimen thickness are not larger than 2.5 $(K_Q/\sigma_{ys})^2$, see section 2.3.1. The measured K_Q values are larger than K_{Ic} values reported in literature, see section 2.3.2. So, to obtain reasonable and valid K_{Ic} values, the specimens need to be fatigue precracked before statically testing.

Table 4.3: The crack length, P_Q and K_Q for the AA6061 specimens with spark-machined notches

Specimen	a (mm)	P_Q (kN)	K_Q (MPa$\sqrt{m}$)	
VN211	17.11	20.0	48.5	invalid
VN212	17.35	16.7	41.3	invalid
VN213	17.88	23.3	60.3	invalid

4.3.2 K_Q Values of Specimens after Fatigue Precracking with a Straight Through Starter Notch

To produce an average K_{Ic} value of AA6061 in T651, B and C condition, two or three replicate tests were executed.
After the heat treatments, the specimens were ground to make the fatigue precrack better visible on the outer surface. The minimum and maximum fatigue precrack lengths were marked on the specimen surfaces. Then, the specimens in T651 condition were fixed in the Schenck servo-hydraulic fatigue machine. This machine was difficult to operate and not accurate, so the specimens in the B and C condition were fatigue precracked with the MTS servo-hydraulic fatigue testing machine. The maximum load was 4 kN and R=0.1. When the fatigue precrack was visible on the outside of the specimen and was long enough, fatigue precracking was stopped. The number of cycles necessary to obtain a fatigue precrack ranged from 111000 to 533000 cycles.
After fatigue precracking, the actual K_{Ic} test was performed with the Instron testing machine. The specimens were fixed in the machine, the clipgauge, see figure 3.2, was placed in the crack mouth and the specimens were torn with a displacement speed of 3 mm/min. A load-displacement diagram could be constructed, from which P_Q was determined as described in section 2.3.1. The crack length, the specimen width and thickness were measured and with equations 2.4 and 2.5, K_Q was calculated. To determine if the calculated K_Q values were valid K_{Ic} values, the validity criteria, as described in section 2.3.1 should be met. All the K_Q values turned out to be invalid since the fatigue crackfronts were too oblique.
In table 4.4, the crack length, P_Q and K_Q are given.

Table 4.4: The crack length, P_Q, and K_Q for the AA6061 specimens with a straight through starter notch

Specimen	a (mm)	P_Q (kN)	K_Q (MPa$\sqrt{m}$)	
T631	17.91	8.7	22.3	invalid
T632	17.66	13.2	32.8	invalid
T633	18.52	11.7	31.8	invalid
B31	19.46	9.9	29.0	invalid
B32	20.04	7.4	23.1	invalid
B33	18.74	*		
C31	21.34	*		
C32	19.98	6.2	18.9	invalid

* the beginning of the load-displacement diagram was curved which made it impossible to determine P_Q

It was concluded that the straight through starter notch caused a lot of obliqueness. The fatigue crack did not initiate on both sides at the same time and this caused the invalidity of the K_Q values. With equation 3.1 and 3.2 the amount of obliqueness and tunnelling were determined, see table 4.5.

Table 4.5: The obliqueness and tunnelling of the fatigue crack front

specimen	crack length (mm)	obliqueness (%)	tunnelling (%)
T631	17.96	21.2	3.9
T632	17.10	23.1	4.2
T633	19.43	11.1	3.0
B31	20.12	19.4	21.7
B32	20.05	30.7	20.2
B33	18.42	17.0	25.6
C31	21.12	8.0	23.8
C32	19.82	7.9	29.2

The fracture surfaces of the specimens in the three different heat treatment conditions show quite distinct features as can be seen in figures 4.10 to 4.12. In T651 condition, the unstable crack growth regions of the fracture surfaces have except for the shearlip regions, no large height differences. The fatigue crack growth regions of the fracture surfaces show lines parallel to the crack growth direction. These lines are due to the fact that small fatigue cracks start at slightly different planes from the main crack plane and grow towards the main crack plane.

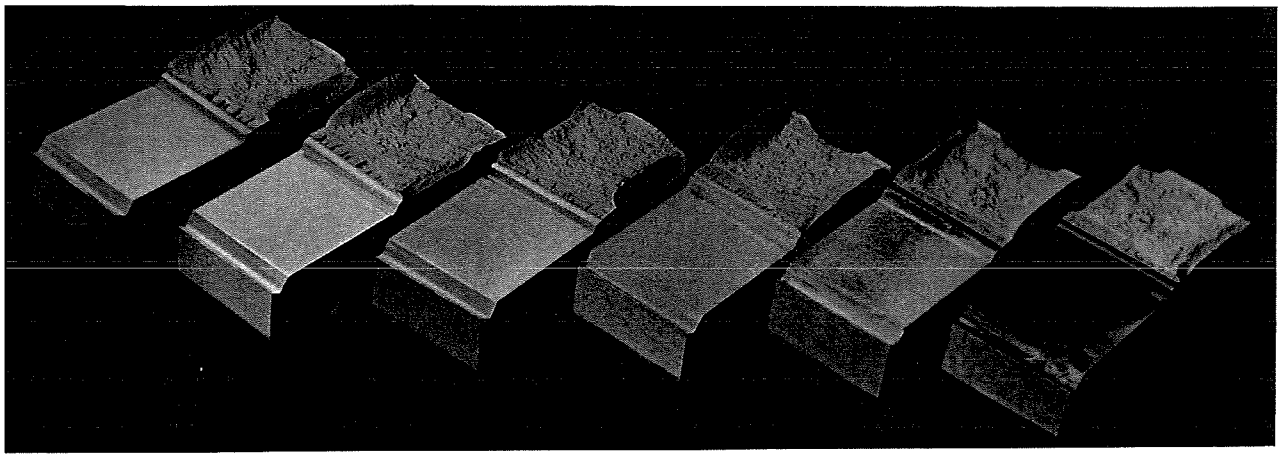

Figure 4.10: The broken specimens after the K_{Ic} test in T651 condition

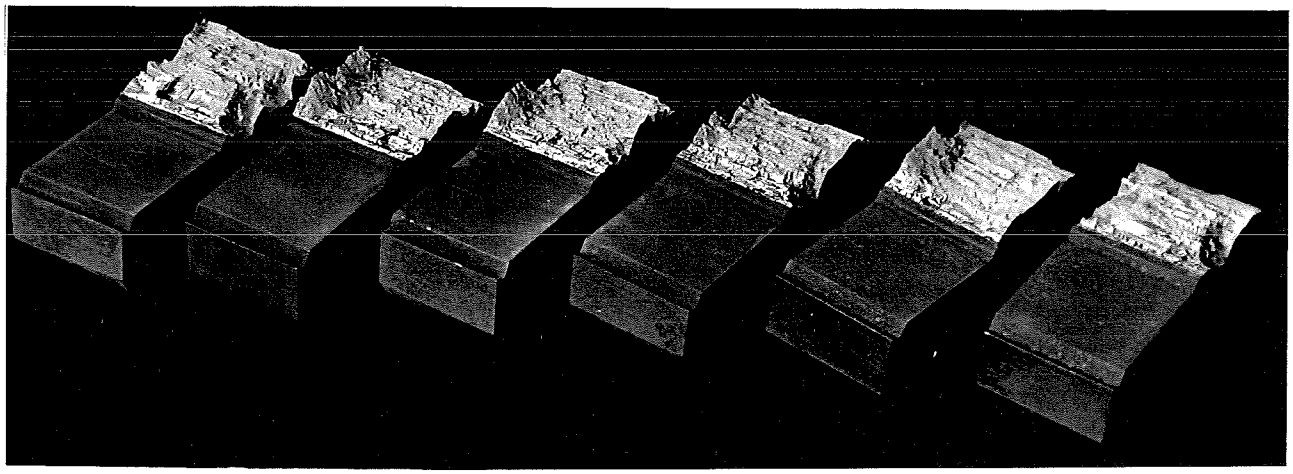

Figure 4.11: The broken specimens after the K_{Ic} test in B condition

The fracture surfaces of the specimens in B condition are much rougher than those of the specimens in T651 condition. In the unstable crack growth region small shearlips are present. The fatigue crack growth region has a glistering appearance with a lot of "steps" perpendicular to the crack growth direction. These steps are probably due to changes in orientation of the main crack plane during crack growth.

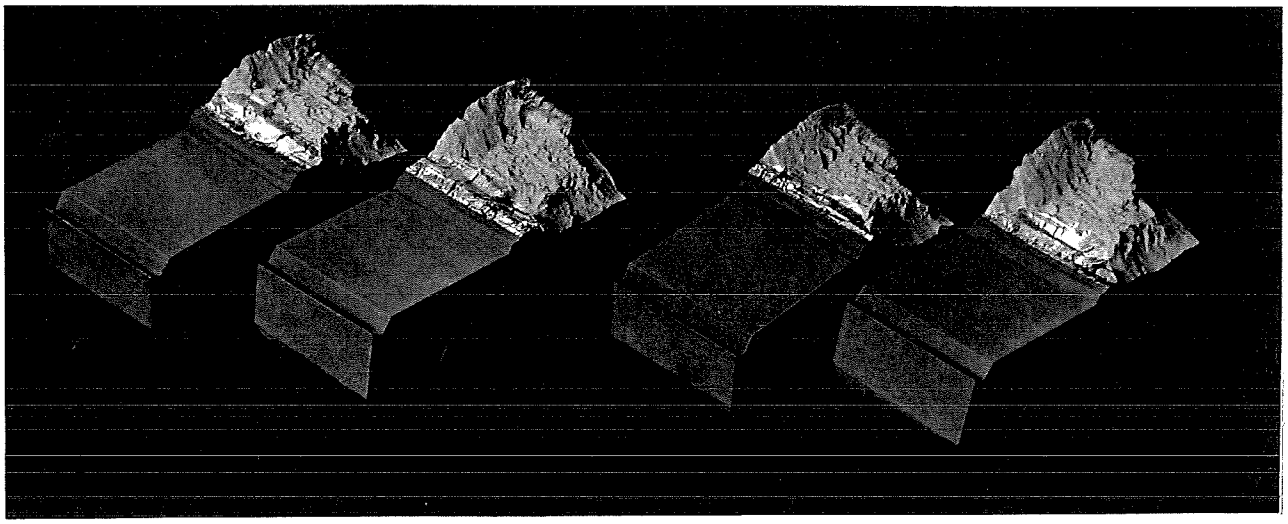

Figure 4.12: The broken specimens after the K_{Ic} test in C condition

The fracture surfaces of the specimens in C condition are also quite rough. The unstable crack growth region has large shearlips, more than 50% of the unstable crack growth region consists of shearlips.
The fatigue crack growth region has a glistering appearance and has "steps" perpendicular to the crack growth direction, like for condition B. These steps are larger than those found in the specimens in condition B. The main crack plane orientation changes considerably during crack growth. Parallel to the crack growth direction lines are visible as in the specimens in T651 condition.

The fracture surfaces were also investigated with a scanning electron microscope. The used acceleration voltage was 2.5 kV. In figures 4.13 to 4.18 the fracture surfaces of specific regions are shown.

Figure 4.13 shows a typical fatigue crack surface.
The unstable crack growth region of the fracture surface consists of larger and smaller dimples, see figure 4.14. This indicates ductile failure as is to be expected with this aluminium alloy. Small precipitates act as nucleation sites where voids can nucleate, see section 2.4. The large dimples range from 3-15 μm. The small honeycomb like dimples in between the large dimples are 1 μm and smaller

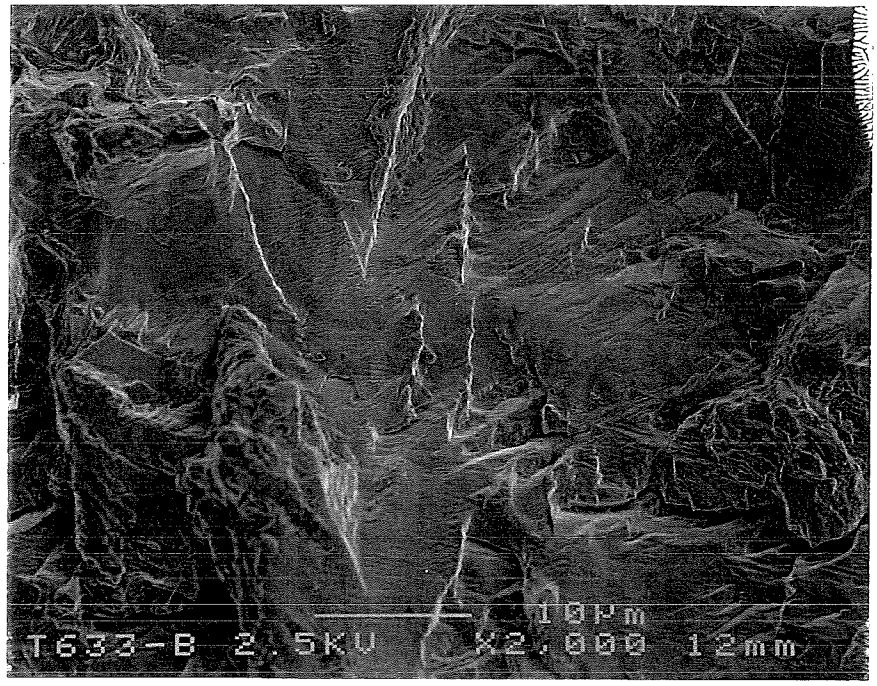

Figure 4.13: Fatigue crack growth region of a specimen half in T651 condition; magnification is 2000x; crack growth direction is from bottom to top

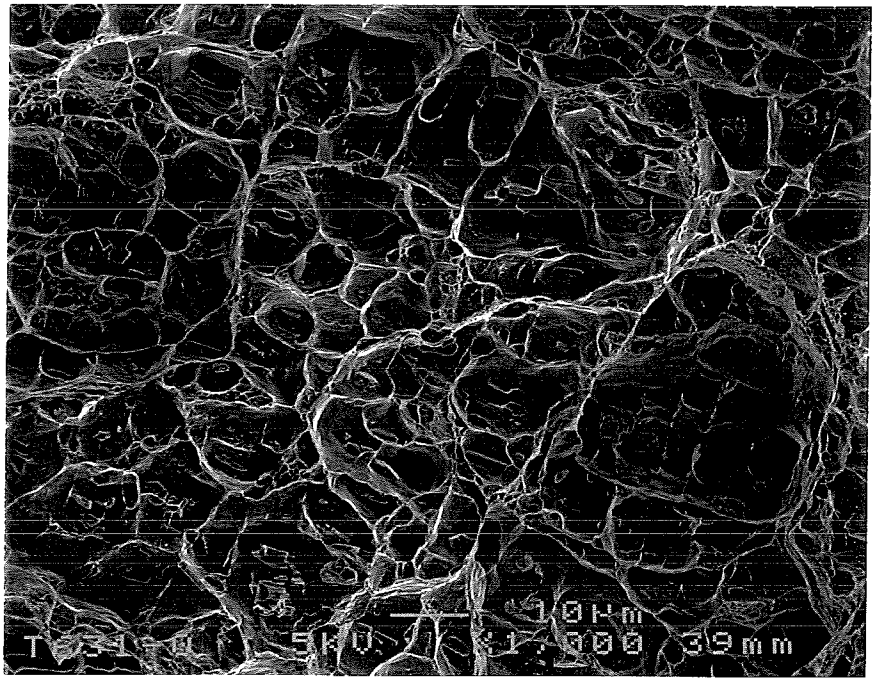

Figure 4.14: Unstable crack growth region of a specimen half in T651 condition; magnification is 1000x, crack growth direction is from bottom to top

In figure 4.15, the transition between the fatigue and unstable crack growth region can be seen of a specimen half in condition B. The fatigue crack growth region is some what less rough in B condition than in T651 condition, the ridges are less high. The unstable

crack growth region consists of dimples as in T651 condition. In B condition some bands with very small dimples in between bands with larger dimples can be seen, see figure 4.16. The large dimples are 5-30 μm, the small ones are 1 μm and smaller.

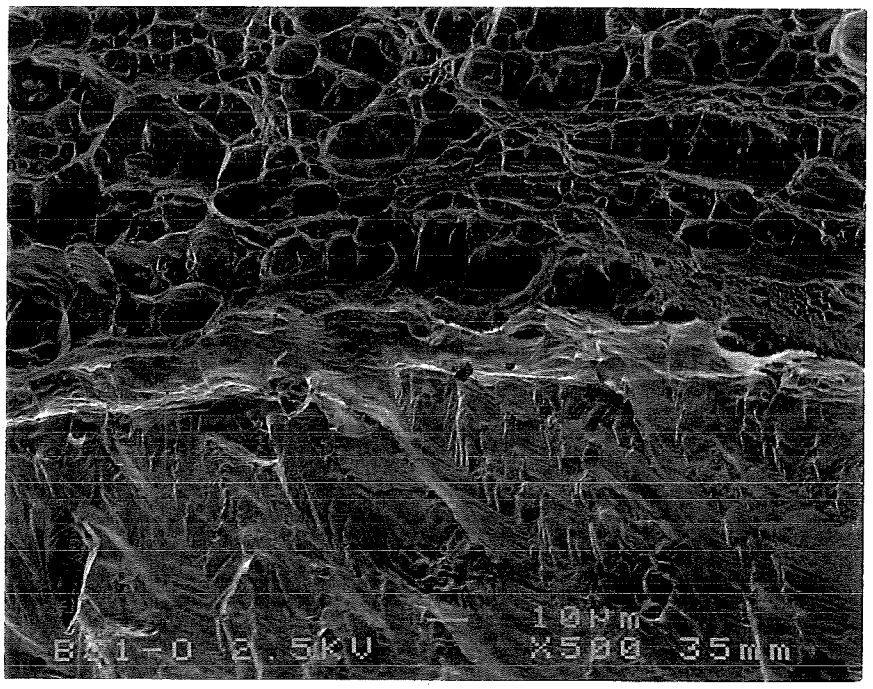

Figure 4.15: Transition between fatigue and unstable crack growth region in B condition; magnification is 500x; crack growth direction is from bottom to top

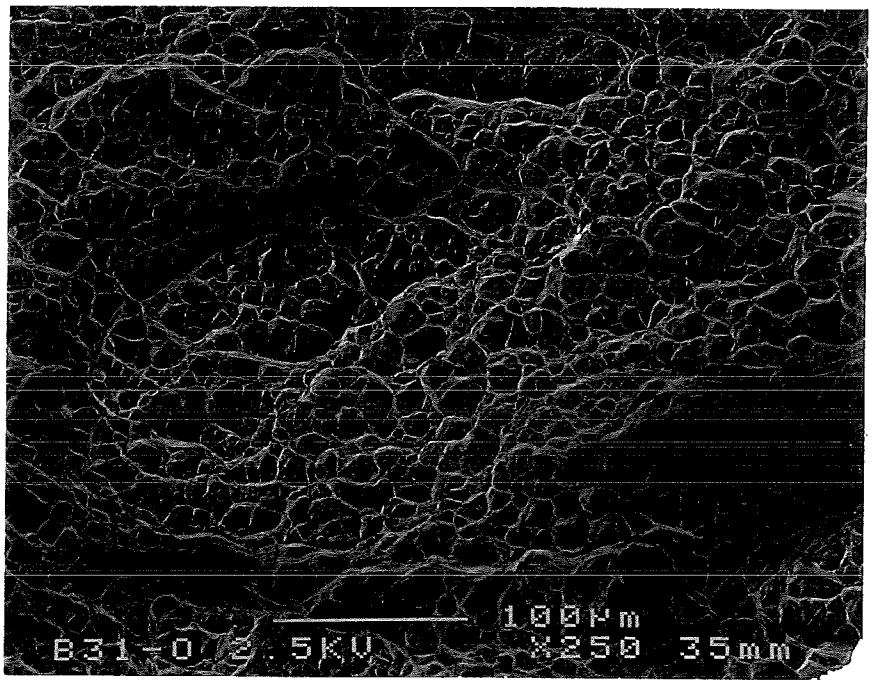

Figure 4.16: Unstable crack growth region in a specimen in B condition; magnification is 250x; crack growth direction is from bottom to top

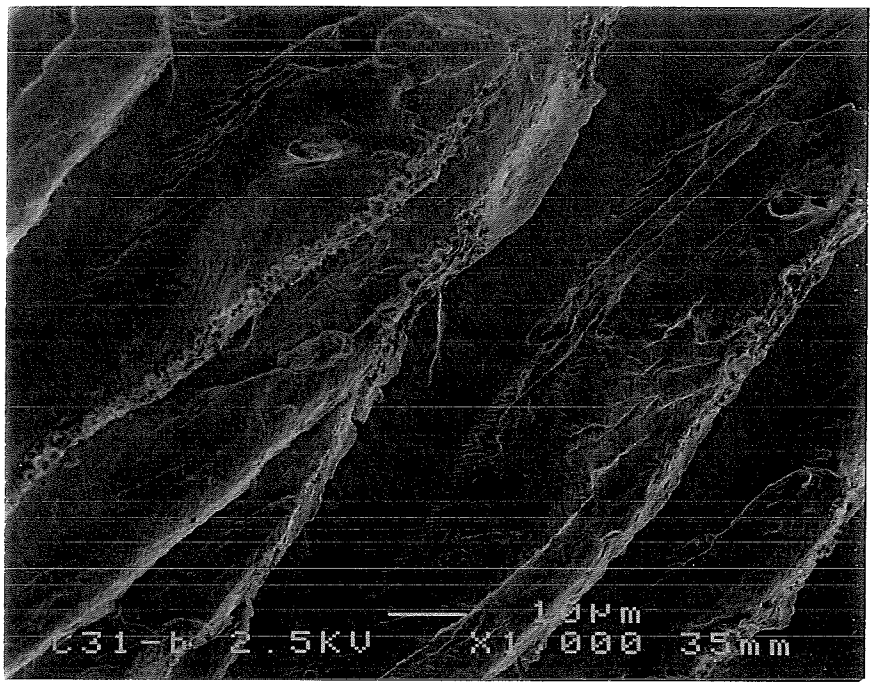

Figure 4.17: Fatigue crack growth region in C condition; magnification is 1000x, crack growth direction is from bottom to top

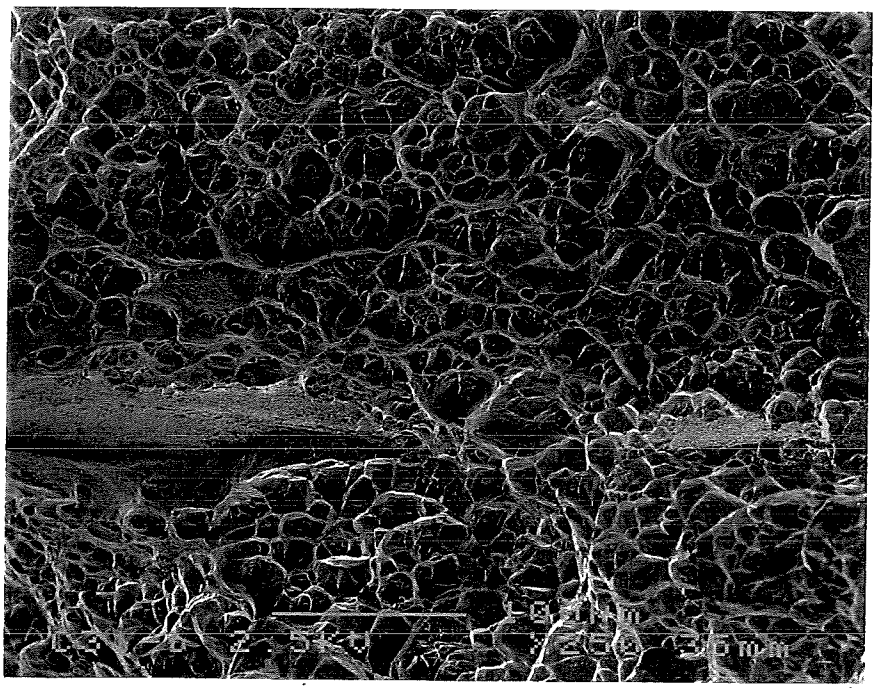

Figure 4.18: Small dimples between larger dimples in the unstable crack growth region in C condition; magnification is 250x; crack growth direction is from bottom to top

In figure 4.17, the fatigue crack growth region of a specimen in C condition can be seen. Large ridges are visible with smooth surfaces in between these ridges. The fatigue crack growth regions in the different conditions are alike, but the structure seems the finest in T651 condition.
The unstable crack growth region in C condition had larger dimples compared with the other two conditions: 7-30 μm. There were small zones with small dimples (1 μm and smaller), like a spider's web between leaves, see figure 4.18.

4.3.3 K_Q Values of Specimens with a Chevron Starter Notch

Because the K_Q values of the specimens with the straight through starter notch were all invalid, also specimens with a chevron notch were made and tested [36]. Two replicate tests were made in each heat treatment condition. Fatigue precracking was done on the MTS servo-hydraulic fatigue testing machine. To determine the crack length during fatigue precracking, a clip gauge was placed in the crack mouth. With equations 3.3 to 3.7 the crack length during fatigue precracking can be determined by measuring the maximum and minimum CMOD and the maximum and minimum load after a certain number of cycles.
In table 4.6 the values of P_Q, a and K_Q are shown [36].

Table 4.6: The crack length, P_Q, and K_Q for the AA6061 specimens with a chevron notch [36]

Specimen	a (mm)	P_Q (kN)	K_Q (MPa$\sqrt{m}$)	
T651-1	16.61	17.5	40.7	invalid
T651-2	16.27	18.7	42.2	invalid
B-1	17.03	19.8	47.6	invalid
B-2	16.74	18.8	44.0	invalid
C-1	16.72	11.6	27.2	invalid
C-2*	21.86	NA*	NA*	

*due to a flaw made during testing, the data was not stored properly
* NA means not available

In the first five tests the crack length was invalid, because the fatigue crack did not emerge on both specimen surfaces. The Young's modulus used in equation 3.6 was much too high leading to overestimation of the crack length during fatigue precracking.

5. RESULTS OF AA6061 MATRIX COMPOSITE

5.1 Chemical Composition of the AA6061 Matrix Composite

The composition of the matrix of the AA6061 composite material was determined with X-ray fluorescence, and is given in table 5.1.

Table 5.1: The composition of the AA6061 material in weight percentage

Mg	Si	Fe	Cu	Cr	Mn	Ti	Zn	Pb	Ni	Al
1.11	0.45	0.05	0.23	0.09	0.001	0.01	0.003	0.008	0.006	rest

The chemical composition is within the limits of AA6061, compare table 5.1 and 3.1, whereby the matrix contains a low percentage of iron and other impurities.
The reinforcement for this mmc consists of angular Al_2O_3 particles with a large range of particle diameters, the average diameter is 20 μm.

5.2 K_{Ic} tests

5.2.1 Fatigue Precracking (Dynamical Part of the Test)

After the various heat treatments as described in section 3.2, the samples were fatigue precracked. During fatigue precracking, the ratio of P_{min}/P_{max} was 0.1.
First the specimens in T6 condition were tested. The maximum load at the end of fatigue precracking is not allowed to exceed 60% of the K_{Ic}. Because the K_{Ic} of metal matrix composites found in literature ranges from 11.1 to 24.2 MPa$\sqrt{m}$ see section 2.3.2, the maximum load to start with was 2kN. After 127150 cycles the maximum load was raised to 3 kN. After 157430 cycles at 3 kN the crack was not visible and the load was increased to 4 kN.
After a while the load was enhanced to 5 kN and the specimen broke after 46100 cycles with 5 kN, because the crack had not been detected on the specimen surface before fracture.
The maximum load at the beginning of fatigue precracking the second specimen in T6 condition was 3 kN. After 118280 cycles there was no crack visible, so the maximum load was raised to 4 kN. After 122670 cycles there was no crack visible but the specimen was removed to prevent fracture during fatigue precracking.
While fatigue precraking the third specimen in T6 condition, a clip gauge was used to measure the CMOD. It was not yet possible to calculate the compliance enhancement as the crack grew. This was due to the fact that the signals gave a lot of noise and the strain gauge turned out to be not calibrated correctly. The crack was not visible and not yet measurable but after 122670 cycles with P_{max} is 4 kN the fatigue precracking was stopped.

After the specimens in T6 condition the specimens in B condition were fatigue precracked. During fatigue precracking the first two specimens in B condition the system to calculate the crack length from the compliance was still not working properly, although the noise was lowered by placing an RC-filter between the output signal and the datalogger. The reason for the inability to monitor the crack growth was that the

CMOD at maximum and minimum load was measured. Measuring this way leaves crack closure, see section 3.4.2, unaccounted for.
The first specimen in B condition fractured during fatigue precracking. The second specimen in B condition (DurB2) was removed after 58160 cycles with P_{max} is 2 kN, 96140 cycles with P_{max} is 3 kN and 394680 cycles with P_{max} is 4 kN.
Meanwhile the system to determine the crack length from the compliance was working.

During fatigue precracking the third specimen in B condition (DurB3) the compliance was measured and the crack length calculated from the compliance, with equations 3.7 and 3.8, with an interval of approximately 30000 cycles. The maximum load during fatigue precracking was 4 kN. In figure 5.1 the crack length against the number of cycles for specimen DurB3 can be seen.

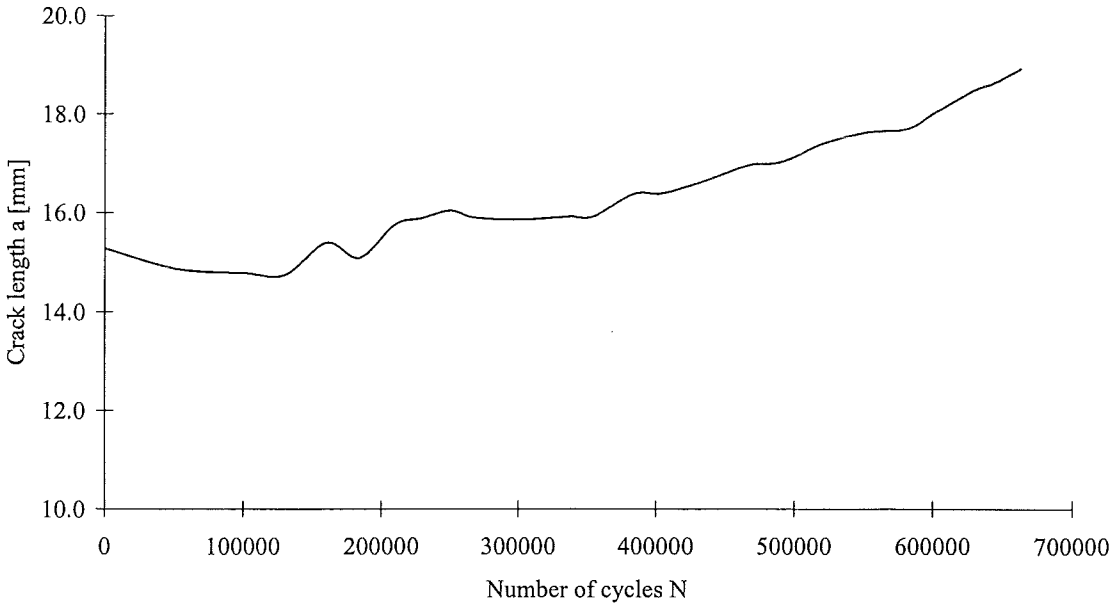

Figure 5.1: The crack length against the number of cycles during fatigue precracking

Fatigue precracking was stopped when the calculated crack length was 18.9 mm.

Fatigue precracking of the first two specimens in C condition was without problems. The maximum load used for all three specimens in C condition was 4 kN and near the end of precracking 3 kN.
Fatigue precracking of specimen DurC1 and DurC2 was stopped when the calculated crack lengths were 20.0 mm and 20.1 mm respectively.

The last specimen in condition C, DurC3, did not fit smoothly in the grips of the fatigue testing machine. The specimen pen holes and the grips had to be ground and enlarged, and the pens ground and polished before the specimen fitted.
Fatigue precracking was stopped when the calculated crack length was 20.2 mm.

5.2.2 Determination of K_{Ic} (Statical Part of the Test)

In table 5.2 the crack length, P_Q and K_Q of the AA6061 matrix composites are listed. Only one of the K_Q values was valid. The K_Q values of the specimens in B condition and specimens DurT64 and DurC2 were invalid because the crack was not through the

whole chevron notch yet. The ratio of P_{max}/P_Q exceeded 1.10 for specimen DurT63 and DurT64.

Table 5.2: Crack length, P_Q and K_Q of the AA6061 matrix composite

Specimen	crack length (mm)	P_Q (kN)	K_Q (MPa$\sqrt{m}$)	
DurT63	18.24	5.9	16.2	invalid
DurT64	15.11*	7.0	14.2	invalid
DurB2	17.23*	8.1	20.6	invalid**
DurB3	17.67*	7.6	20.2	invalid**
DurC1	18.96	7.2	22.4	invalid**
DurC2	18.84	6.9	20.9	invalid**
DurC3	18.43	7.4	21.4	valid**

* The fatigue precrack did not initiate throughout the whole specimen width

**The σ_{ys} of the Duralcan material in the B and C heat treatment conditions have to be estimated as these values were not measured.

The crackfronts were a bit oblique and tunnelled but only the K_Q of specimens DurC1 and DurC2 were invalid because of too much tunnelling.

The specimen halves were investigated in the SEM, see figure 5.2 to 5.7. The first specimen half, the one in T6 condition, was ultrasonic cleaned. The acetone was gray after ultrasone cleaning, so probably some particles were trilled from the fracture surface. To control if particles were trilled out another specimen half in T6 condition was not ultrasone cleaned and investigated in the SEM. The acceleration voltage used for the mmc material was 15 kV.
Special attention was focussed on the amount of particles in the fatigue and unstable crack growth region of the fracture surfaces in the different heat treatment conditions.

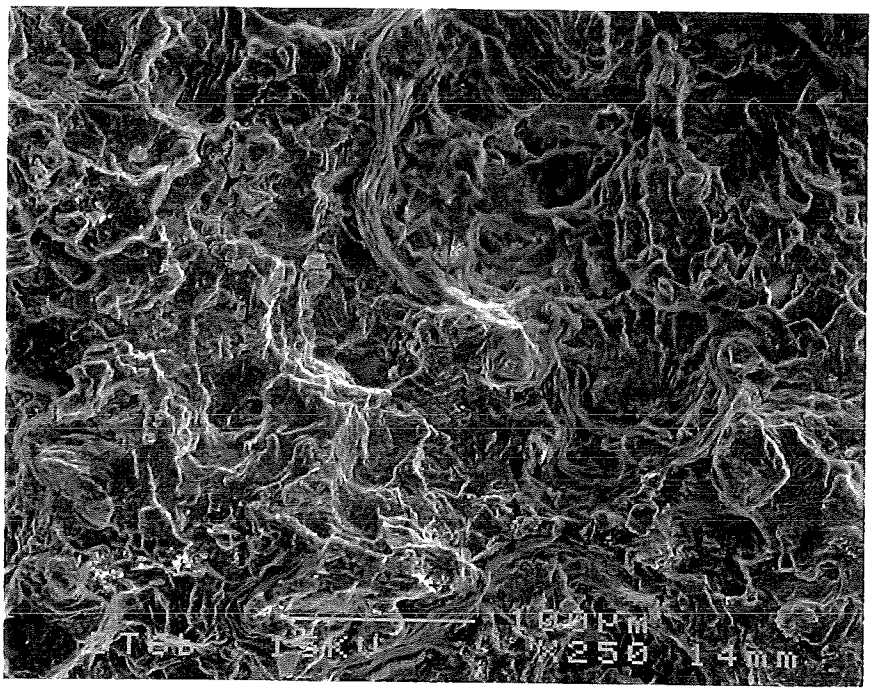

Figure 5.2: Fatigue crack growth region of a specimen half in T6 condition; magnification is 250x; crack growth direction is from bottom to top

The fatigue crack growth region shows some distinct features. The fatigue structures are coarse. Notice that there are only a few particles visible on the fracture surface, while the material consists of 20 vol.% Al_2O_3 particles.

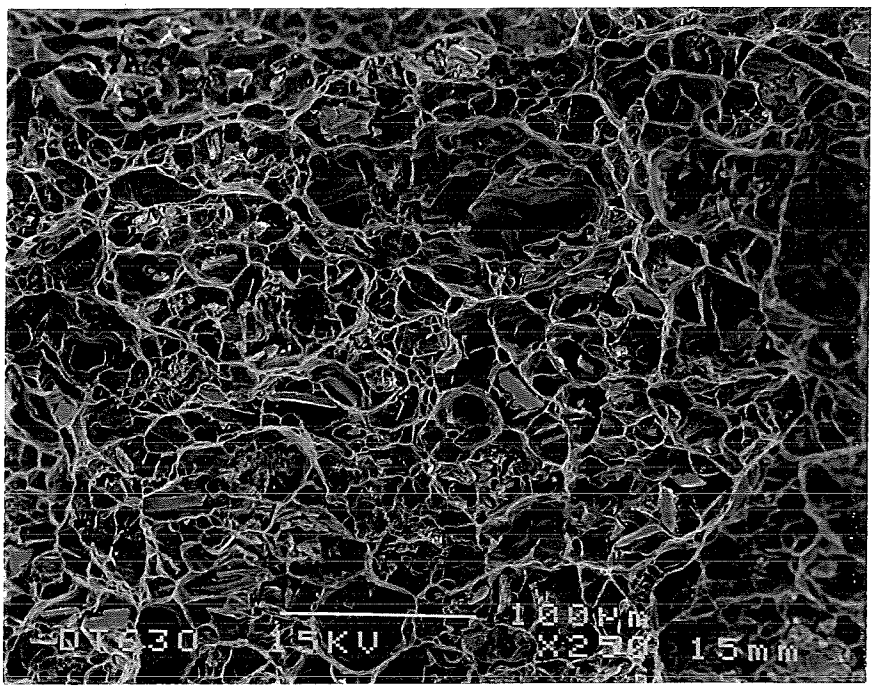

Figure 5.3: Unstable crack growth region of a specimen half in T6 condition; magnification is 250x; crack growth direction is from bottom to top

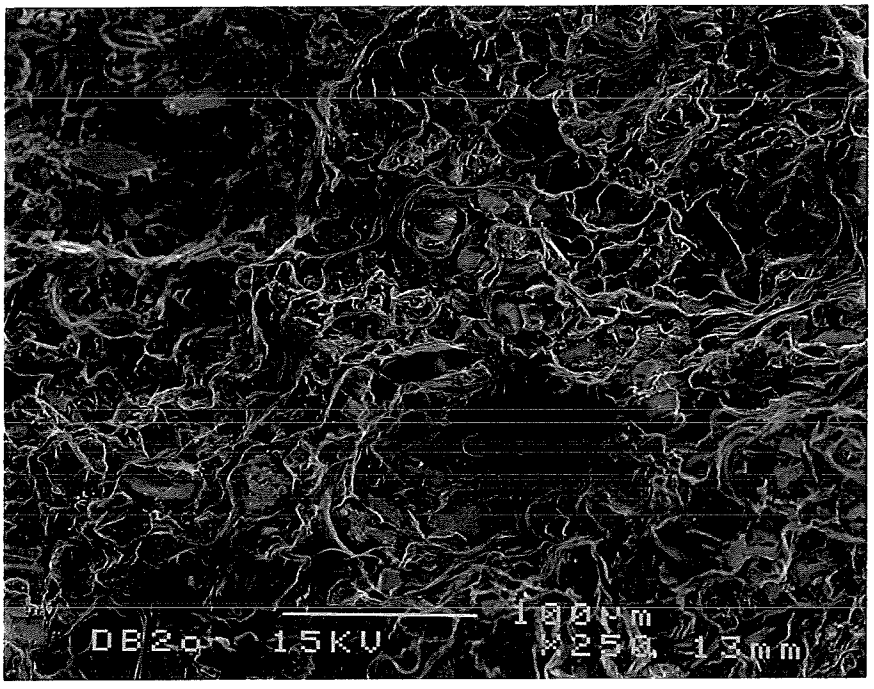

Figure 5.4: Fatigue crack growth region of a specimen half in B condition; magnification is 250x; crack growth direction is from bottom to top

In the unstable crack growth region of the specimens in T6 condition a lot of particles are visible, see figure 5.3. Larger particles are broken. Around the particles dimples have formed. Some large dimples appear to be empty. In between the large dimples around the particles, smaller dimples (< 10 μm) are visible.

As can be seen in figure 5.4, the fatigue crack growth region in B condition shows more particles on the fracture surface then the same region in T6 condition.
In the unstable crack region even more particles are visible on the fracture surface, see figure 5.5.

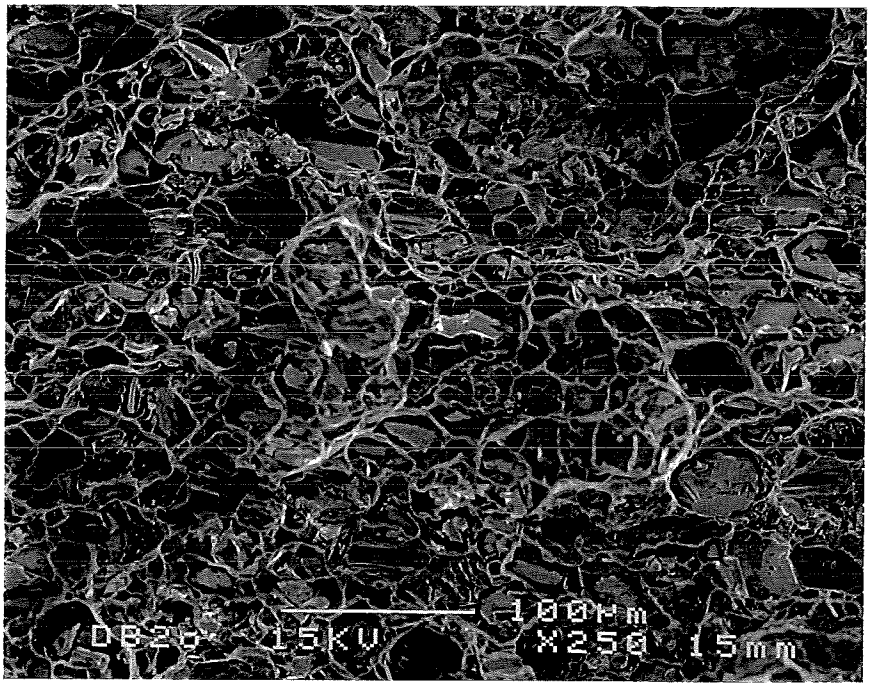

Figure 5.5: Unstable crack growth region of a specimen half in B condition; magnification is 250x; crack growth direction is from bottom to top

The fracture surface of the unstable crack growth region shows a lot of particles lying in large dimples (10-40 μm). In between the large dimples around the particles, smaller dimples (<10 μm) can be found.
The fatigue crack growth region in C condition shows more particles then in T6 condition but less then in condition B, see figure 5.6.

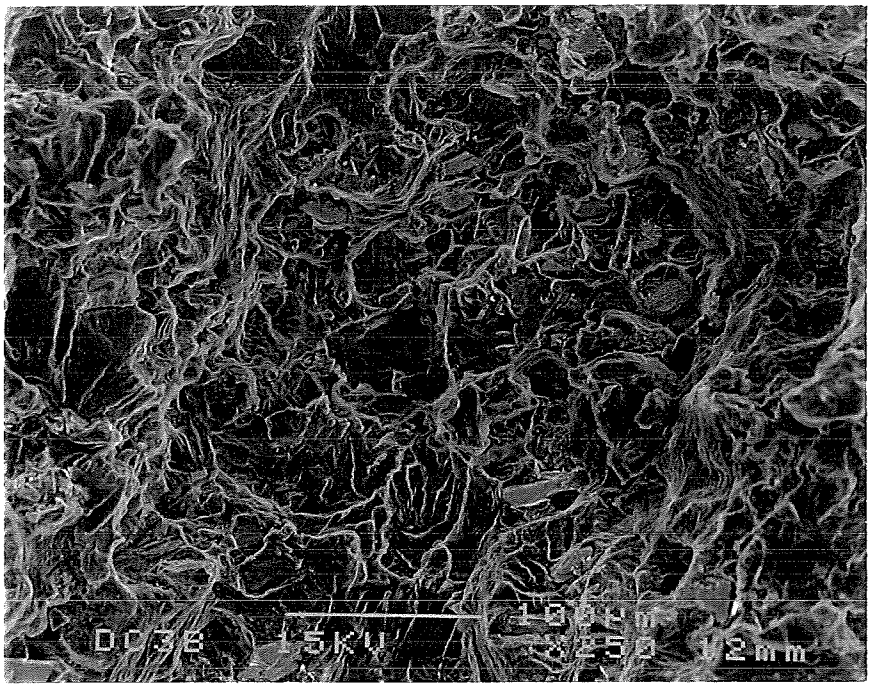

Figure 5.6: Fatigue crack growth region of a specimen half in C condition; magnification is 250x; crack growth direction is from bottom to top

The unstable crack growth region in C condition looks the same as the unstable crack growth region in B condition, see figure 5.7.

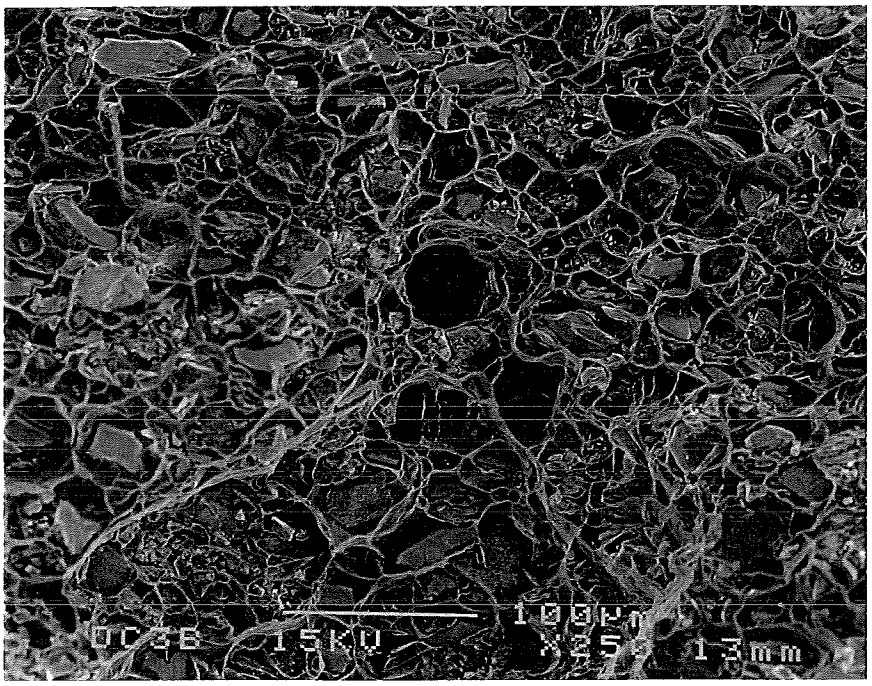

Figure 5.7: Unstable crack growth region of a specimen half in C condition; magnification is 250x; crack growth direction is from bottom to top

To make a comparison of the fracture surfaces in the different heat treatment conditions, the number of particles visible on a SEM photo in the fatigue and unstable crack growth region are counted. Two SEM photos, with magnification 250x, of both the unstable and fatigue crack growth region were taken in the three conditions. The results of the particle counts are listed in table 5.3.

Table 5.3: The amount of particles counted on SEM photos of the fracture surface with a magnification of 250x (c.g.r. is crack growth region)

	Fatigue c.g.r.	Fatigue c.g.r.	Unstable c.g.r.	Unstable c.g.r.
DurT63	3	9	45	47
DurB2	33*	38	96	99
DurC3	16	15	105	98

*height differences in the fracture surface caused a very dark part on the photo leading to a possible underestimation of the number of particles

5.3 Mg Enrichment

In all heat treatment conditions Mg enrichment in the particle/matrix interface is visible, as can be seen in figures 5.8 to 5.11.

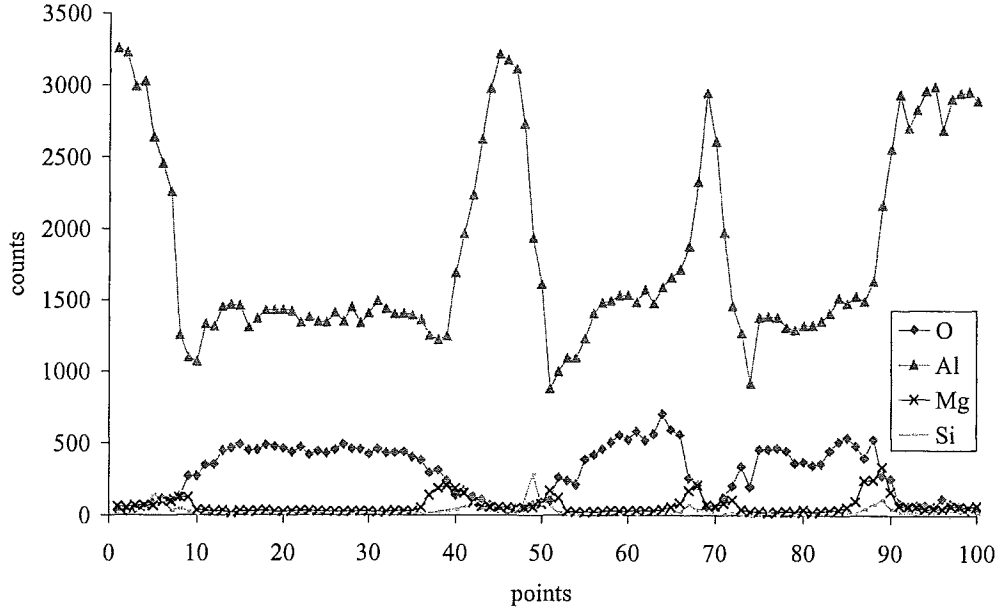

Figure 5.8: Linescan of AA6061 based mmc with 20 vol.% Al_2O_3 particles in T6 condition

The particles can be recognised by the increase of oxygen and the decrease of aluminium. As described in section 3.6 the amount of an element can only regarded relative to itself. Adjacent to every particle a zone with more Mg than the surroundings is visible. With X-ray mapping the outlines of the particles are visible in the aluminium, oxygen and magnesium map, see figure 5.9.

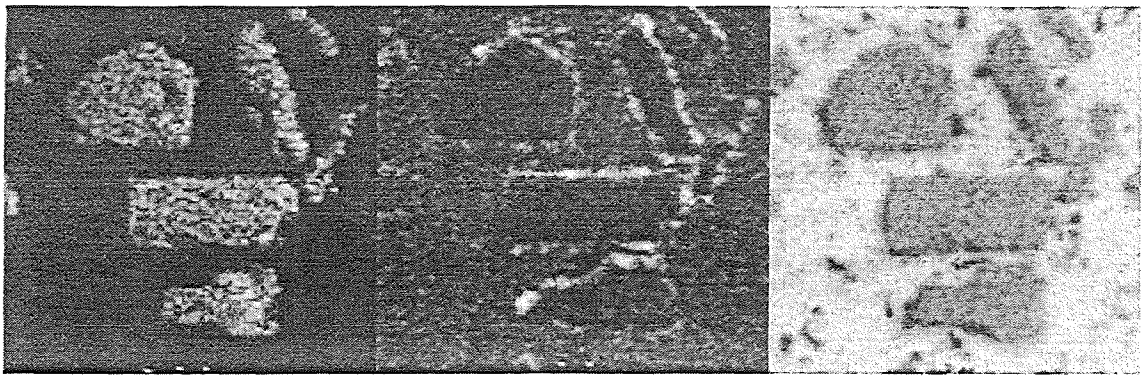

a) b) c)

Figure 5.9: X-ray maps of a) oxygen, b) magnesium and c) aluminium

In the X-ray maps higher concentrations are brighter than lower concentrations. In the particles there is less Aluminium, so the X-ray map of aluminium shows darker particles. The oxygen level is much higher in the particles (Al_2O_3) than in the matrix, so the particles are visible as brighter parts in the oxygen X-ray map. It is difficult to say something about silicon because the samples are ground, whereby silicon carbide can be pushed in the soft matrix material.

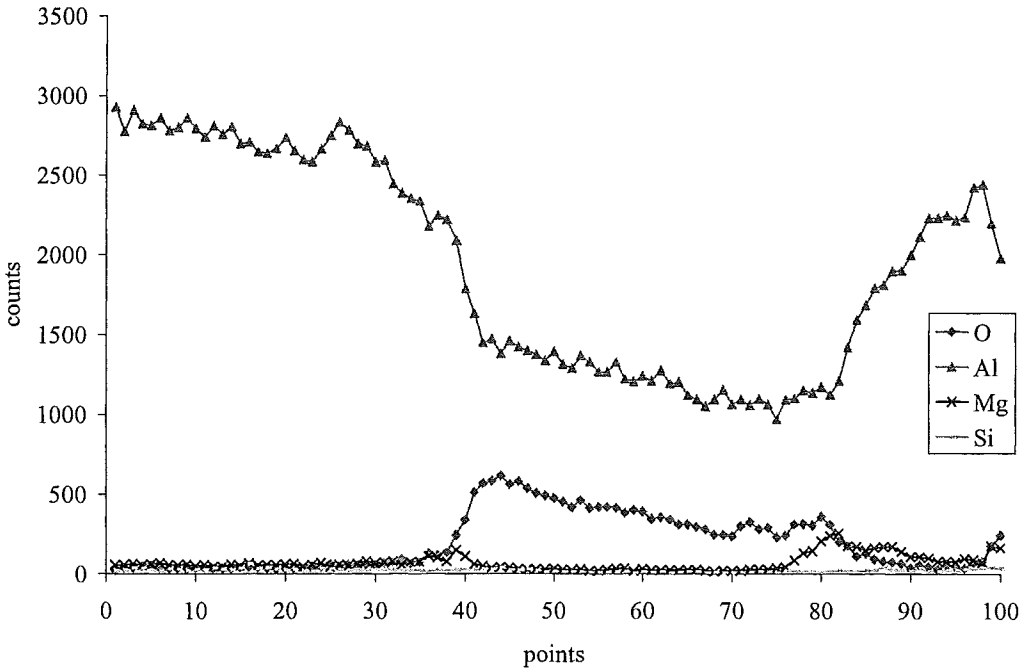

Figure 5.10: Linescan of AA6061 based mmc with 20 vol.% Al_2O_3 particles in B condition

In figure 5.10 just one particle can be seen. The Mg enrichment is visible adjacent to the particle.

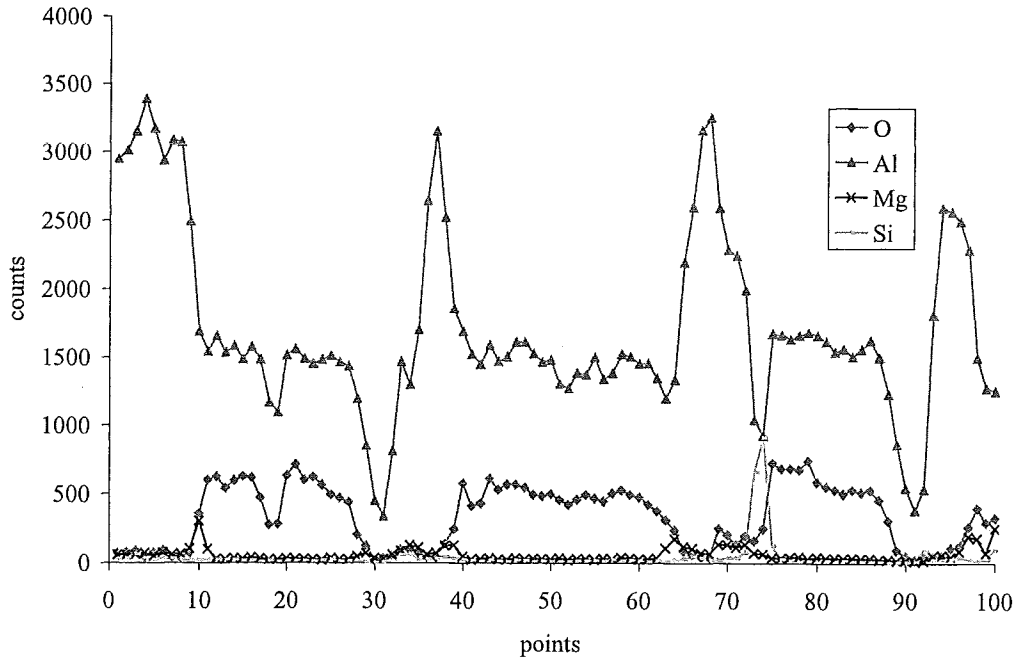

Figure 5.11: Linescan of AA6061 based mmc with 20 vol.% Al_2O_3 particles in C condition

The linescan of the sample in C condition shows a large silicon peak (point ~73) due to a silicon carbide particle of the grinding paper. The Al_2O_3 particles are clearly visible. Some Mg enrichment next to the particles can be discerned. In between two particles a bit of matrix material is ground away, visible as a large decrease in aluminium (point ~30 and point ~90). In those two spots the counts of oxygen, magnesium and silicon also decrease supporting the idea of matrix loss in those two points. During SEM investigation of the samples in C condition a lot of scratches were visible in the matrix.

6. DISCUSSION

6.1 AA6061

6.1.1 Heat treatment

Although different precipitate structures were to be expected, see section 2.2, the microstructures after the different heat treatment conditions seem alike under the light microscope, as can be seen in figures 6.1 to 6.3.

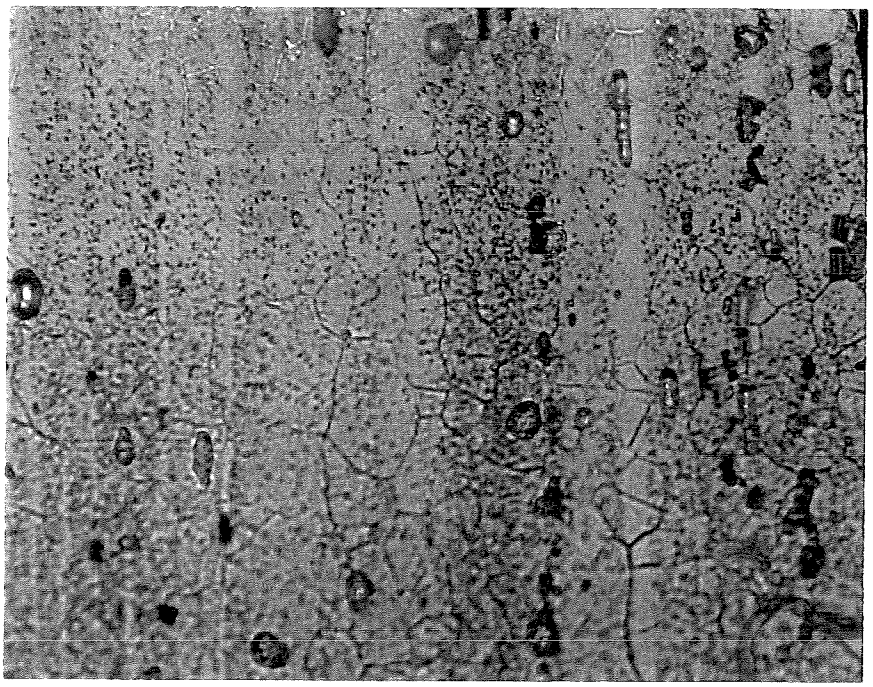

Figure 6.1: AA6061 specimen in the delivered T651 condition perpendicular to the extrusion direction; magnification is 1000x

In T651 condition some very large constituents are observed on the grain boundaries. There is no precipitate free zone next to a grain boundary and the smaller dispersoids are in bands with a higher or lower dispersoid density parallel to the extrusion direction.

Figure 6.2: AA6061 specimen in B condition perpendicular to the extrusion direction; magnification is 1000x

In B condition the dispersoids are homogeneously spread throughout the material, there are very few large constituents, and the ones found are smaller than the large constituents present in T651 condition.

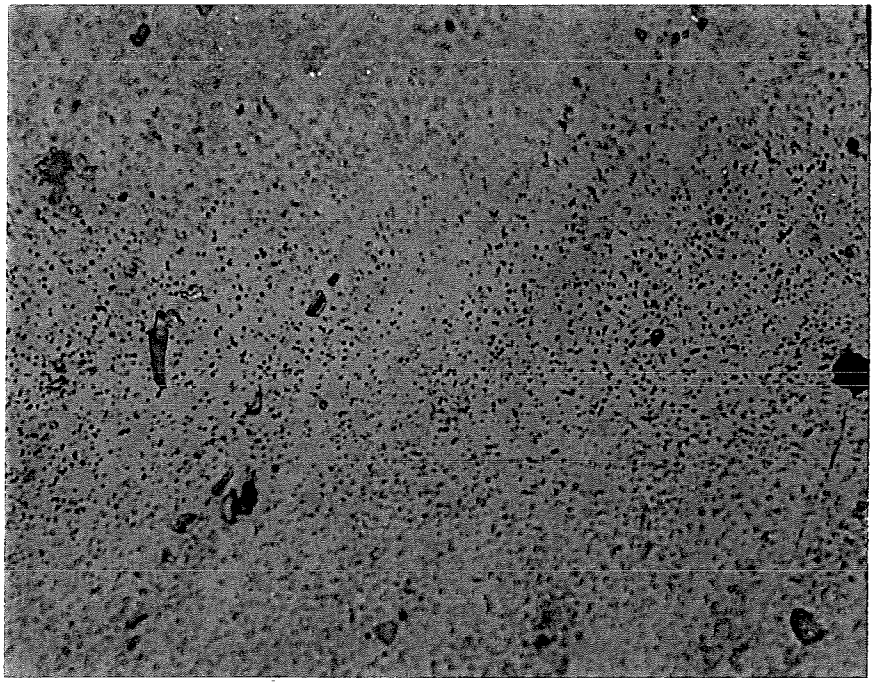

Figure 6.3: AA6061 specimen in C condition perpendicular to the extrusion direction; magnification is 1000x

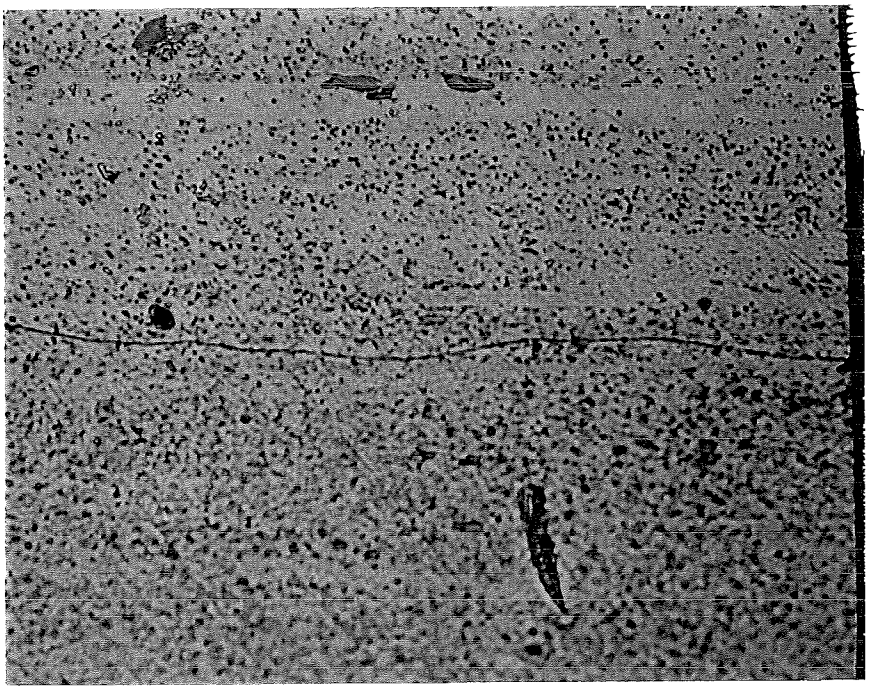

Figure 6.4: AA6061 specimen in self-made T6 condition perpendicular to the extrusion direction; magnification is 1000x

In C condition, see figure 6.3, there are some large constituents, which are a bit smaller and more angular than in T651 condition. These large constituents are not situated at grain boundaries. The small dispersoids are homogeneously spread like in B condition. To see if the large constituents in T651 dissolve during solutionizing, two tensile specimens in delivered condition were given a standard T6 heat treatment. This T6 heat treatment consisted of 2 hrs solutionizing at 530 °C followed by water quenching and ageing for 8 hrs at 175 °C. The tensile specimens were tested, see section 6.1.2 and from the tested specimens, samples for microstructure and grain size investigations were taken
The microstructure of the self-made T6 condition is shown in figure 6.4. The microstructure looks similar as B and C condition, with dispersoids homogeneously spread throughout the material and some large angular constituents.

During heat treatment B only β" precipitates are expected to have formed, and only β' precipitates during heat treatment C, see sections 2.2 and 3.2. The specimens in T651 condition are expected to have a mix of β" with some β' precipitates. These precipitates are very small in the order of 0.01-0.05 μm. The β" precipitates are only visible by strain contrast in Transmission Electron Microscopy (TEM) [37, 38]. The only way to verify the assumptions made about the present precipitates after the different heat treatments, is to investigate the specimens with TEM. As that is a difficult and very time consuming technique and out of the scope of this investigation, this was not done.
The particles visible in figures 6.1 to 6.4 are obviously too large to be the hardening β" or β' precipitates. In AA6061 other alloying elements play a role in determining the microstructure. Iron is an impurity that is assumed to form β-(FeSi)Al plate like constituents that are detrimental to the toughness of AA6061. Under the influence of Cr and Mn the β-(FeSi)Al can be transformed during heat treatment in α-(FeMnSi)Al. The

iron containing constituents are relatively large (> 1μm). The large angular constituents in figures 6.1 to 6.4 could be the iron containing constituents as described above.
Cr and Mn can also form small (0.05-0.25 μm) incoherent dispersoids. These incoherent dispersoids prevent recrystallisation during heat treatment. They also have a toughening effect on AA6061 [39]. This toughening is a result of grain refinement and the fact that dispersoids are not sheared by dislocations. The dislocations pile up at each dispersoid and harden each active slip plane, which causes slip to be transferred to adjacent planes [37].
The copper in the AA6061 can lead to grain boundary precipitates influencing the corrosion resistance. The small dispersoids visible in figures 6.1 to 6.4 are probably those Cr or Mn rich dispersoids.
The large round particles in figure 6.1 are investigated in the SEM, whereby pointscans were made. They appeared to be very large Mg and Si containing precipitates, this indicates that the material was cooled very slowly after solutionizing or solutionizing was not done long enough.

The grains are much larger in B, C and self-made T6 condition than in T651 condition. To compare the grain sizes, the specimens were etched anodic, thus making the grains visible under polarised light. In figures 6.5 to 6.8 the grain sizes can be seen. The microscope specimens for the self-made T6, B and C condition are taken from the threaded ends of the tensile test specimens. This means that the specimens show a plane perpendicular to the extrusion direction. The specimen used for the delivered T651 condition was taken from the delivered material in the same direction.

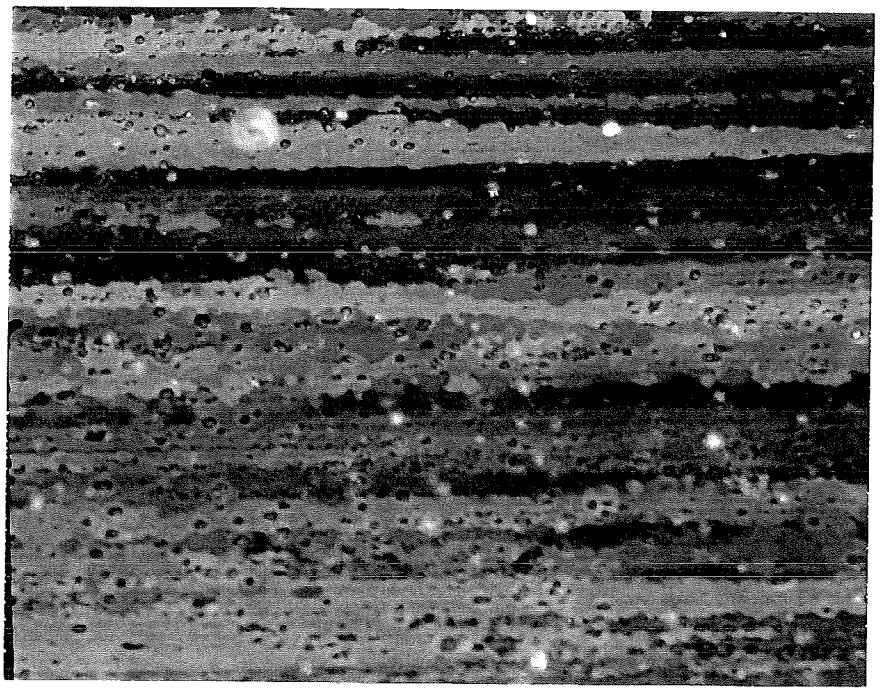

Figure 6.5: AA6061 specimen in T651 condition, extrusion direction is horizontal; magnification is 200x

In T651 condition the grains are very long in the extrusion direction and very small perpendicular to the extrusion direction, as can be seen in figure 6.5.

Figure 6.6: AA6061 in B condition, the extrusion direction is horizontal; magnification is 25x

On the edge of the specimens in B and C condition some very small grains are visible. To the centre of the specimen the grains become larger. The grains are elongated in the extrusion direction.

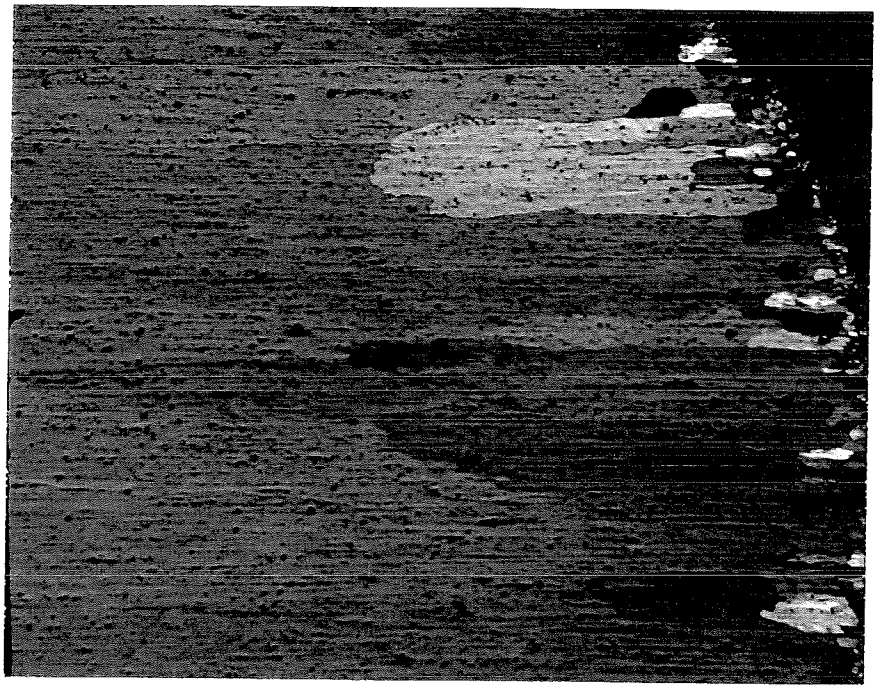

Figure 6.7: AA6061 in C condition, the extrusion direction is horizontal; magnification is 25x

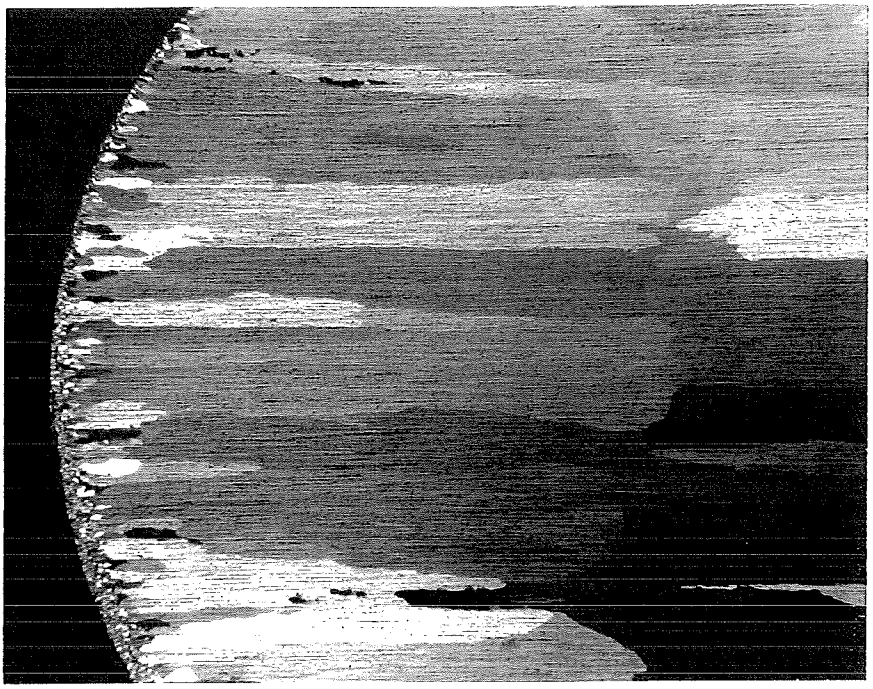

Figure 6.8: AA6061 in the self-made T6 condition, the extrusion direction is horizontal; magnification is 16x

In all conditions the grains are elongated in the extrusion direction, but the grain thickness is much larger in the specimens which have had a heat treatment in the laboratory. On the edge of the microscope samples, taken from the end of the tensile specimens, some recrystallisation is visible. This may have occurred during machining the threaded ends or during solutionizing. The larger grain sizes in the direction perpendicular to the extrusion direction are due to grain growth during solutionizing.

6.1.2 Tensile Tests

In the stress-strain curve of specimen 6061-1 (figure 4.1) a kink can be seen in the transition from elastic to plastic deformation. This kink is very unlikely to occur and indicates a flaw in the test. Therefore this specimen will be kept out of further discussion.

Several differences can be seen between the different heat treatments. The strain hardening exponent is much larger in C condition, whereas the yield stress is much lower. These facts can be explained as follows. The hardening precipitates in C condition are much larger than in B condition and T651. This means that there are fewer obstacles to pin the dislocation movement. This leads to a lower yield stress. During the tensile tests more obstacles for dislocation movement are formed. These obstacles themselves consist of dislocations, which leads to strain hardening.
Overall, the stress-strain curves of C condition resemble an overaged material.

B condition is the condition in which the material is strongest and shows very little necking. The delivered T651 condition is tougher than B and C condition. It is less strong than B condition. Regarding the stress-strain curves, it might be expected that the

precipitation structure of condition T651 is a mixture of the precipitates in B condition and C.
The fracture surfaces of the tensile specimens in T651 condition show cups. This indicates that fracture occurred by internal voiding. This means that the crack starts in the centre of the specimen when voids nucleate and coalesce. These voids can nucleate on the large precipitates on the grain boundaries, see figure 6.1. Macroscopical shearing is difficult because of the grain boundaries and the large incoherent precipitates.

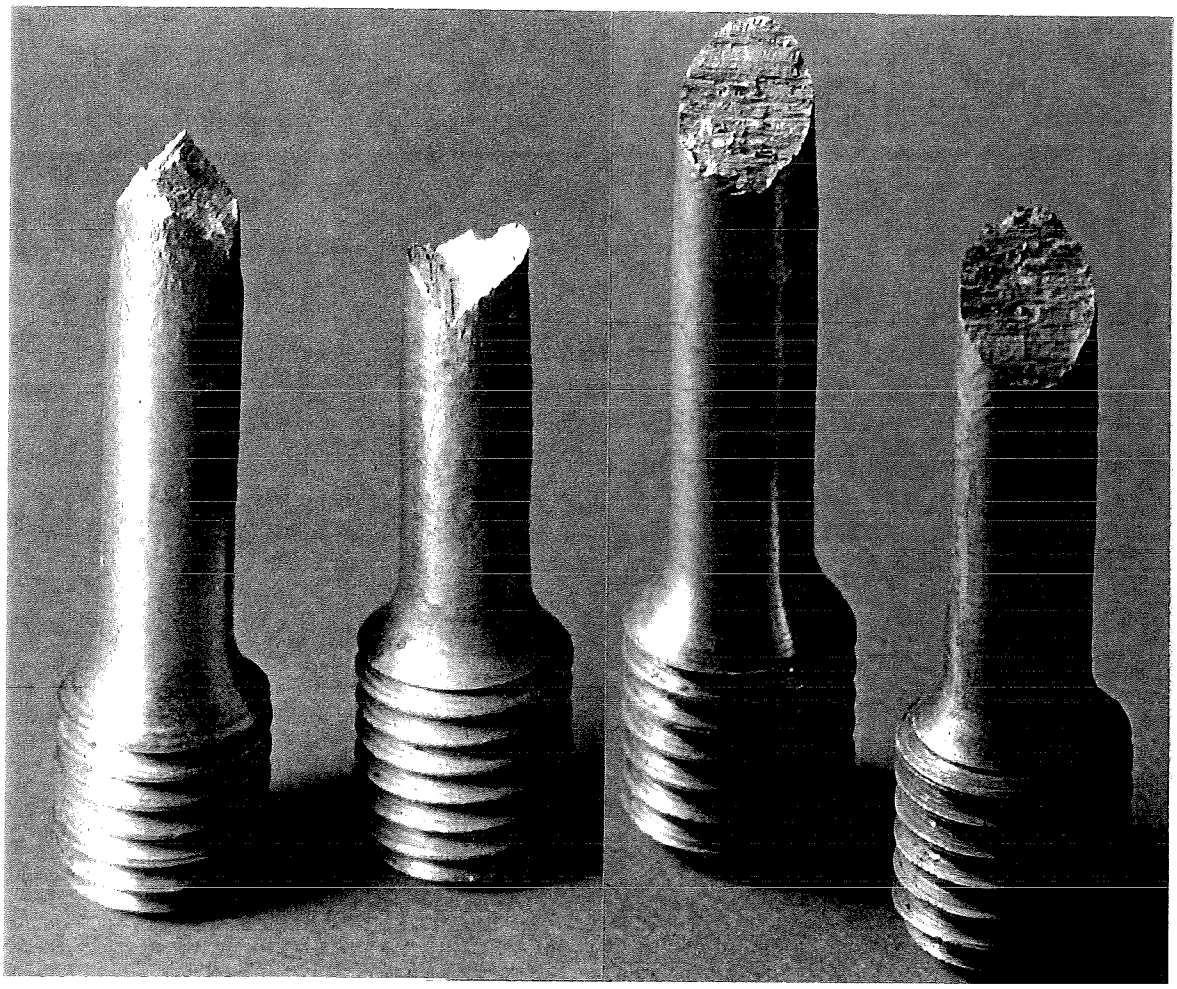

Figure 6.9: Broken tensile specimens in self-made T6 condition

The specimens in B, C and self-made T6 condition show an incline fracture plane at an angle of ~ 45° to the specimen surface, indicating a shear mechanism. The maximum shear stress acts in that plane and causes shear fracture. The fracture mode of the tensile specimens in the self-made T6 condition was also shear fracture, see figure 6.9. There are few grain boundaries and less or no large incoherent precipitates on the grain boundary. So there are little obstacles for shearing.

In table 6.1 the Young's modulus, the yield stress, the ultimate tensile strain and the work hardening exponent of the specimens in self-made T6 condition are given.

Table 6.1: Material properties determined with tensile test on specimens in self-made T6 heat treatment

specimen	E (GPa)	σ_{ys} (MPa)	ε_{uts} (%)	n
6061T6-1	66.9	336	10	0.087
6061T6-2	73.0	347	11	0.090

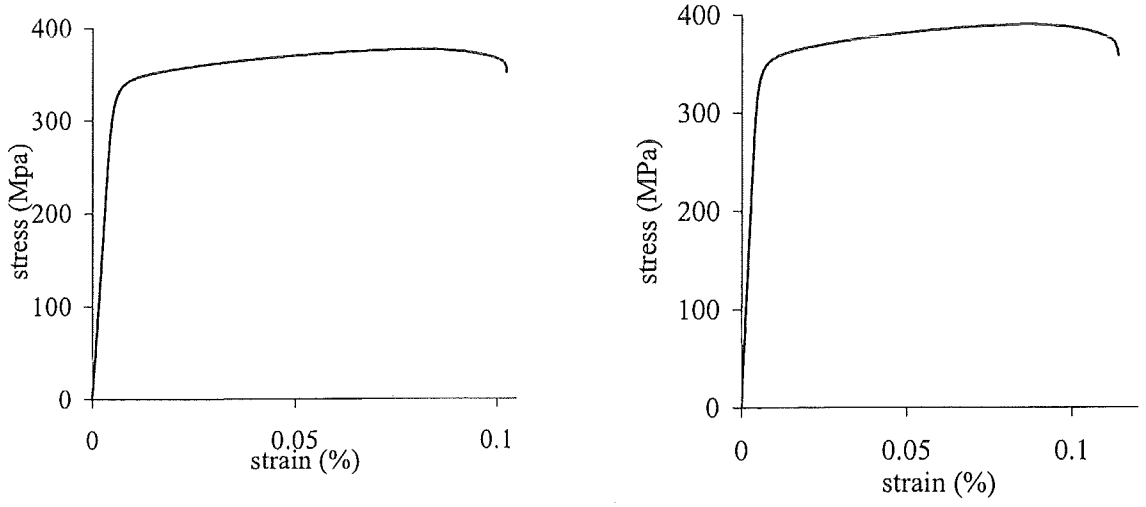

Figure 6.10: Stress-strain curves of AA6061 in self-made T6 condition

When comparing these values with the values in table 4.1 and figure 6.10 with 4.1 and 4.2, the yield stress, ultimate tensile strain and work hardening exponent are similar to the specimens in B condition. The delivered T651 condition seems to be tougher than the self-made T6 condition.

6.1.3 K_{Ic} Tests

None of the performed K_{Ic} tests was valid according to requirements specified in the ASTM standard [23], although specimen geometry was altered twice.
First the specimens with the spark-machined notches led to incredible high K_Q values. The notch was not sharp enough to assume that the crack tip radius is essentially zero, see section 2.3.1 and since the stress intensity analysis in section 2.3 is not valid for blunt cracks, this leads to an overestimation of the K_{Ic}.

The specimens with fatigue precracked notches were invalid mostly because of crack tunnelling and obliqueness.
In T651 condition the crack fronts were oblique, the crack started at one surface and did not straighten during fatigue crack growth. In B condition the shear lips were smallest and the fatigue crack front was both tunnelled and oblique. In C condition the tunnelling was most severe. The tunnelling might be caused by internal residual stresses that can arise from quenching the specimens from 309°C to room temperature. This would also explain why the tunnelling is most severe in C condition. T651 and B condition are quenched from 175°C and 256°C respectively giving rise to lower residual stresses in the specimens. Extensive crack tunnelling can lead to plane stress conditions instead of plain strain conditions during the actual K_{Ic} test. The material can deform in the thickness direction, especially the material near the surface of the specimen.

The steps visible in the fatigue crack growth regions of all conditions can be linked to the grain size in the direction perpendicular to the extrusion direction. In every grain there is a preferable crack plane, the crack follows that plane until the grain boundary is reached, than it changes to the preferable plane in the next grain. In T651 condition the grains are small (0.01-0.05 mm) in the direction perpendicular to the extrusion direction

leading to small steps, which are too small to be measured accurately with the used measure microscope. The grain sizes in that direction in B and C condition are much larger leading to larger steps. The step sizes in B and C condition are 0.3-0.9 mm, whereby the measured grain sizes are 0.2-0.7 mm, see figures 6.5 and 6.6.

The chevron notch should have led to valid K_{Ic} values. However this was not the case, because the fatigue precrack length was too short. The fatigue precrack length was calculated from the CMOD measurements, see equations 3.6 to 3.8. The used Young's modulus during the first five measurements was much too high leading to an overestimation of the crack lengths. This was corrected before the last specimen was fatigue precracked, the fatigue crack length of this specimen is valid but the data storage during the actual K_{Ic} test failed.
The crack fronts in the specimens with the chevron notches are less oblique and tunnelled than the crack fronts in the specimens with the straight through notches.
In C condition the shear lips are again very large, larger than the shear lips on the fracture surfaces of T651 and B condition.

Regarding all fracture surfaces, AA6061 in C condition seems most ductile, because of the large shear lips. This contradicts the K_Q values that indicate that the T651 and B condition are more ductile. The load displacement diagrams of the specimens with straight through as well as chevron notches in C condition show curvature in the beginning of the load displacement. In B condition a bit of curvature is seen in the beginning of the load displacement diagram. This curvature can indicate yielding or stable crack growth [40, 41]. The large shear lips might have formed during plastic collapse of the ligament.

Microscopically seen the dimple size is larger in B and C condition than in T651 condition. In conditions with less precipitates the voids have a chance to grow before they coalesce with other voids. In T651 condition a lot of large precipitates on the grain boundaries are visible, these large precipitates will lead to voids that can not grow a lot before they coalescence. In B and C condition there are less of these large precipitates, so voids arising around these precipitates can grow before coalescence. This explains the fact that the dimples in T651 condition are smaller than in B and C condition.

6.2 AA6061 Matrix Composite

6.2.1 Fatigue Precracking

The specimens in T6 and B condition show oblique crack fronts. As the crack measurement during fatigue precracking did not yet work properly the fatigue precracking was stopped too early, the crack did not emerge on both specimen surfaces. The crack fronts of the specimens in C condition were tunnelled too much, leading to invalid K_Q values.

To predict the crack length during fatigue precracking, the Young's modulus and the specimen thickness need to be known or estimated, see equations 3.6 and 3.7. The Young's modulus is not very susceptible for heat treatments, only 6 % difference in unreinforced AA6061, see section 4.2, the reinforcement in the mmc will lead to a higher Young's modulus and a smaller influence of the heat treatment. So the Young's modulus of the mmc can be taken as a constant for the three different heat treatments. The Young's modulus as given by Alcan Aluminium Corporation is 98 GPa [23]. The specimen thickness has been measured for one specimen and was 19.81 mm, the thickness of the other specimens were measured after testing. After testing the specimen, the real crack length at the end of fatigue precracking can be measured, with these values and equations 3.6 and 3.7 the Young's modulus can be calculated. In table 6.2 the predicted and calculated or measured values of the Young's modulus, the specimen thickness and the crack length are given.

Table 6.2: The predicted and calculated or measured values of the parameters in equations 3.6 and 3.7

specimen	predicted E (GPa)	calculated E (GPa)	predicted B (m)	measured B (m)	Predicted a (m)	measured a (m)	flaw in a (%)
C1	98	88.8	0.01981	0.019431	0.02002	0.020017	0.015
C2	98	82.7	0.01981	0.019488	0.02013	0.019647	2.4
C3	98	77.5	0.01981	0.019390	0.02019	0.019195	4.9
B3	98	82.3	0.01981	0.019365	0.01892	0.018264	3.5

Although the Young's modulus was overestimated by more than 10%, the predicted crack length is in good agreement with the measured crack length. This is due to the fact that the logarithm of the Young's modulus is used, this reduces the relative flaw to 3.0 % or less.
The average calculated Young's modulus is 82.8 GPa, with these few values it is not possible to verify the assumption that the Young's modulus is constant for the different heat treatments.

6.2.2 K_{Ic} tests

Although there is only one valid value, the invalid K_Q values give a good indication of the K_{Ic} for the investigated mmc. Specimen DurT64 is left out of further discussion because the crack length was too short and the crack front only covered 60% of the

specimen thickness. The other specimens merely failed the requirements. The K_Q values are highest in C condition and lowest in T6 condition.

The fracture surfaces of the specimens in T6 condition show very few particles in the fatigue part of the crack. The crack avoids the particles and the particle/matrix interface and goes through the matrix material, thereby creating a very rough fatigue crack growth region. During fatigue precracking an ideal crack plane with essentially zero crack tip radius needs to be achieved, see section 2.3.1. A rough fatigue precrack leads to a lower stress intensity at the crack tip. P_Q will therefore be higher than in the flat crack that is necessary to obtain a K_{Ic}. So the K_Q of the specimens in T6 condition will be an overestimation of the K_{Ic}.
In the unstable crack growth region more particles are visible on the crack surface. The material fails in the particle/matrix interface and in the matrix. Some larger particles are cracked, the matrix material is strong enough to load the particles to their fracture stress. The flaw probability in the particles enhances with particle size thus decreasing the particle fracture stress, the larger particles fracture more easily. As any arbitrary plane in the mmc material should consist for some 20% of particles, there is no obvious preference of the crack to go through particles, matrix or interface.

In B condition the fatigue crack growth region shows more particles than the T6 condition. The crack goes through matrix and particle/matrix interface, it is difficult to see if particles are also cracked. Some larger particles cracked perpendicular to the crack plane. The fatigue properties of the material are a mix of particle, matrix and interface fatigue properties.
In the unstable crack growth region, a lot of particles are visible. Much more than 20% of the fracture surface is covered by particles. This means that the matrix material is strong enough to load the particles or the particle/matrix interface to their fracture stress. As there are little empty dimples produced during debonding, the particles are loaded to their fracture stress. The dimples around the particles are large probably indicating debonding of the particle/matrix interface perpendicular to the fracture plane.

The fatigue crack growth region in C condition shows some particles, more than in T6 but less than in B condition. Less than 20% of the fatigue crack growth surface is covered by particles, indicating a preference of the crack for the matrix.
In C condition the fatigue crack growth region shows a lot of particles, comparable with the unstable crack growth region in B condition.

The Mg enrichment in the particle/matrix interface was visible in all three heat treatment conditions. The matrix in C condition was more damaged during grinding and polishing. Because all grinding and polishing is done manually, grinding forces are not constant. Therefore, it is not valid to conclude that the matrix in C condition is softer than the matrices in T6 and B condition.
In some cases silicon enrichment in the particle/matrix interface was also visible. It is not possible to deduct if Mg_2Si is present in the interface, this would require pointscans instead of linescans. In contrast to linescans, pointscans can reveal the amount of elements relative to each other, see section 3.6.

In section 2.5 the Hahn and Rosenfield model is described, the parameters necessary to calculate the K_{Ic} with this model are listed below.

particle diameter D, as determined by Alcan Aluminium Corporation [23] ~ 20 μm
Young's modulus E, as calculated see table 6.2 ~ 82.8 GPa

yield stress σ_y, as determined by finite element modelling [42] ~ 300 MPa
volume fraction V_f, as determined by Alcan Aluminium Corporation [23]~ 20%

The calculated K_{Ic}, using equation 2.8, is ~37 MPa$\sqrt{m}$, this much higher than the measured K_{Ic}.
A possible explanation for the overestimation of the K_{Ic} is that the volume fraction of particles in the fracture surface is higher or lower.
The Hahn and Rosenfield model calculates the K_{Ic} of material with particles homogenously distributed through the material. In figures 5.2 to 5.7 it can be seen that the crack front shows little particles in the fatigue crack growth regions and more particles in the unstable crack growth regions. In a homogenous material the crack can deflect towards or from particles. If the crack deflects towards the particles the volume fraction in the crack plane is higher than the average volume fraction, this happened in the unstable crack growth regions of B and C condition. This would lead to a lower λ in equation 2.6. For example if the amount of particles in the crack plane is 60%, the predicted K_{Ic} drops to 31 MPa$\sqrt{m}$.
This model predicts an enhancement of the fracture toughness with particle size. This contradicts other researches [3, 4, 5] in which a decrease in fracture toughness with particle size due to a higher flaw probability in larger particles is found, see section 2.1.1.

6.3 Comparing AA6061 with AA6061 Matrix Composite

The rise of the Young's modulus with 20 vol.% of Al_2O_3 is low, compare 82.8 GPa with the average Young's modulus of AA6061, 75 GPa. The measured Young's modulus is considerably lower than the one given in the product information 98 GPa [23]. The Young's modulus is not measured in a standard way, with tensile tests, but indirect by using the compliance measurements. Because the crack length is reasonably good predicted, the Young's modulus will be reasonably reliable.

The yield stress determined for the mmc using finite element modelling, 300 MPa, is lower than that measured in AA6061; this contradicts the general assumption that particle reinforced material is stronger. It was not possible to perform tensile tests on the mmc, because the maximum specimen length was 50 mm. This would lead to a specimen diameter of 5 mm, see section 3.3. Local differences in particle size could lead to early failure in a spot with a large particle, because this particle has a higher flaw probability. Tensile tests on these small specimens would lead to great differences in measured values. Specimens taken in another direction from the mmc rod would not lead to comparable values as K_{Ic} and the tensile tests are all done perpendicular to the extrusion direction.
But if tensile tests were possible the yield stress would probably be higher than the yield stress of AA6061.

The K_{Ic} of the mmc material is lower than the K_{Ic} of AA6061. The K_{Ic} of AA6061 in T6 condition is 26-37 MPa$\sqrt{m}$, see section 2.3.2. The K_Q of AA6061 reinforced with 20 vol.% Al_2O_3 particles in T6 condition is 16 MPa$\sqrt{m}$, this is a decrease of at least 38%. In the other conditions the K_Q is ~20 MPa$\sqrt{m}$, that is at least 26% lower than AA6061 in T6 condition.

The fatigue crack growth regions of AA6061 and AA6061 mmc in T6 condition are alike. Only a few particles are visible on that part of the fracture surface of the mmc.

In B and C conditions more particles are visible in the fatigue crack growth region, but the matrix has the same features as the fatigue crack growth region in AA6061.

The unstable crack growth region shows dimples in AA6061 as well as in AA6061 reinforced with 20 vol.% Al_2O_3 particles. The sizes of the large dimples in the mmc material are governed by the particle size. The dimples are larger in the mmc material than in AA6061 because the particles are 20 μm. The smaller dimples in between the particles are comparable with the dimples in AA6061.

7. CONCLUSIONS

7.1 AA6061

Extensive grain growth during heat treatment makes it difficult to compare the tensile test results of the delivered T651 condition with the B, C and self-made T6 condition. B, C and self-made T6 condition have similar grain sizes and can be compared. The self-made T6 condition is comparable in strength with B condition and B and T6 condition are both stronger than C condition.

Fatigue precracking turned out to be absolutely necessary to obtain a sharp crack tip. The measured K_Q values on the specimens with the straight through starter notches are lower than the values measured on the specimens with the chevron notches, see tables 4.4 and 4.6. The straight through starter notch led to more oblique crack fronts. Crack tunnelling occurred in both straight through and chevron notched specimens and although extensive crack tunnelling can lead to plane stress instead of plane strain conditions, it should be possible to obtain valid K_{Ic} values with the chevron notched specimens.
It is not possible to derive a relationship between the heat treatment condition and the measured K_Q values.

During solutionizing, the large Mg and Si containing precipitates that are present in the delivered T651 condition, dissolve. These large precipitates (still present in the delivered T651 condition) can cause voids in the centre of the tensile specimens, leading to a fracture surface called cups.
The large grains and the absence of large precipitates in B, C and self-made T6 condition led to shear fracture in the tensile specimens. The large grains also led to large steps in the fatigue crack growth region of specimens in B and C condition.
The different hardening precipitates in B and C condition, β" and β' respectively, can not be made visible with a light microscopy.

7.2 AA6061 Matrix Composite

Only one of the K_Q values of the tested mmc material is valid, however the other values give a good indication of the fracture toughness in the different heat treatment conditions. The K_Q of AA6061 with 20 vol.% of Al_2O_3 particles in T6 condition is ~ 15 MPa$\sqrt{m}$.
The K_Q value in B condition is ~ 20 MPa$\sqrt{m}$ and the C condition seems to lead to the highest K_Q value ~ 21 MPa$\sqrt{m}$.
The AA6061 based mmc material has a considerably lower K_Q than the K_{Ic} of unreinforced AA6061 as found in literature, 26-37 MPa$\sqrt{m}$.

In all conditions, much less particles were seen in the fatigue crack growth region than in the unstable crack growth region of the fracture surface. In T6 condition the fatigue crack growth region shows the least particles, in B condition the most.

It is not possible to see whether the particles were broken or decohesion of the particle/matrix interface had occurred on the SEM pictures.

Mg enrichment in the particle/matrix interface was found in all conditions. The formation of $MgAl_2O_4$ spinels in the interface can have its influence on interfacial behaviour.
Because linescans were made it is not possible to determine the amount of Mg enrichment in the different conditions quantitatively. Therefore it is not possible to relate the amount of Mg enrichment in a specific heat treatment with the corresponding K_Q values.

8. RECOMMENDATIONS

The alternative heat treatments used in this investigation, are not yet fully understood. The precipitates formed during heat treatment B and C should be investigated with Transmission Electron Microscopy.
To make a good comparison between the delivered standard T651 and the self-made B and C condition, the experiments should be repeated with specimens with comparable grain sizes. Also the nature of the large precipitates on the grain boundaries in the delivered T651 condition is not known.

There is just one valid K_{Ic} value for the AA6061 based composite, but the alternative C heat treatment seems to lead to a higher fracture toughness. This needs further examination, because higher toughness would ameliorate the applicability of metal matrix composites.

To understand the behaviour of metal matrix composites it is necessary to look at the fracture mechanisms. It would be ideal if it is possible to make a fracture model in which it is possible to predict the fracture mechanisms in mmcs, when matrix, interface and particle properties are known. An idea to investigate whether particles crack or debonding of the particle/matrix interface occurs is to look at it in the SEM using back scattered electrons for imaging.

The Mg enrichment is demonstrated in this investigation but if some pointscans were made, it is possible to determine if there are only $MgAl_2O_4$ spinels or also some Mg_2Si precipitates present in the interface.

LITERATURE

1. Clyne T.W. and Withers P.J., *An Introduction to Metal Matrix Composites*, Cambridge: Cambridge University Press, 1993, pp 1-3.

2. Van Gorp A.C., *Fracture Toughness and Heat Treating of Al6061 Based Metal Matrix Composites*, literature review, Delft, 1997

3. Mortensen A.,'A Review of the Fracture Toughness of Particle Reinforced Aluminium Alloys', eds. Masounave, J. and Hamel F.G., ASM Conference Proceedings: *Fabrication of Particulate Reinforced Metal Composites*, Montreal, Canada, 1990, pp. 217-233.

4. Doel T.J.A. and Bowen P., 'Effect of Particle Size and Matrix Aging Condition on Toughness of Particle Reinforced Aluminium Based Metal Matrix Composites', *Materials Science and Technology*, Vol. 12, July 1996, pp. 586-594.

5. Marchal Y., Delannay F. and Froyen L., 'The Essential Work of Fracture as a Means for Characterizing the Influence of Particle Size and Volume Fraction on the Fracture Toughness of Plates of Al/SiC Composites', *Scripta Materialia*, Vol. 35, No. 5, 1996, pp 193-198.

6. Rabiei A., Kim B.-N., Enoki M. and Kishi T., 'Fracture Behaviour in 6061 Alloy Matrix Composites with Different Reinforcements', *Materials Transactions, JIM*, Vol. 37, No. 5, 1996, pp. 1148-1155.

7. Hadianfard M.J., Healy J.C., and Mai Y.W., 'The Influence of Heat Treatment on Mechanical and Fracture Properties of an Alumina Microsphere Reinforced Aluminium Matrix Composite.' *International Conference on Advanced Composite Materials 1993*, eds. T. Chandra and A.K. Dhingra, 1993, pp.1199-1204.

8. Roebuck B. and Lord L.D., 'Plane Strain Fracture Toughness Test Procedure for Particulate Metal Matrix Composites', *Materials Science and Technology*, Vol. 6, 1990, pp. 1199-1209.

9. Flom Y. and Arsenault R.J., 'Effect of Particle Size on Fracture Toughness of SiC/Al Composite Material', *Acta Metallurgica*, Vol. 37, No. 9, 1989, pp. 2413-2423.

10. Hadianfard M.J., Heness G., Healy J.C., and Mai, Y.W., 'Fracture Toughness Measurements and Failure Mechanisms of Metal Matrix Composites', *Fatigue & Fracture of Engineering Materials & Structures*, Vol. 17, No. 3, 1994, pp. 253-263.

11. Chakraborti N. and Lukas H.L., *Ternary Alloys,* eds. Petzoward G. and Effenberg, G., VCH Publishers, New York, 1993, pp 2-14.

12. Metals Handbook ninth edition, eds W.H. Cubberly, V. Masseria, C.W. Kirkpatrick and B. Sanders, ASM, Vol.4, 1981, pp 697-700.

13. Song Y. and Baker T.N., "Accelerated Aging Processes in Ceramic Reinforced AA6061 Composites', *Materials Science and Engineering,* Vol. 10, May 1994, pp. 406-413.

14. Salvo L. and Sury M., 'Effect of Reinforcement on Age Hardening of Cast 6061 Al-SiC and 6061 Al-Al_2O_3 Particulate Composites', *Materials Science and Engineering,* Vol. A177, 1994, pp. 19-28.

15. Song Y. and Baker T.N., 'A Calorimetric and Metallographic Study of Precipitation Process in AA6061 and its Composites', *Materials Science and Engineering,* Vol. A201, 1995, pp. 251-260.

16. Salvo L, Suéry M. and Descomps F., 'Age Hardening of Al-Matrix Composites Containing Various Types of Reinforcements', ASM Conference Proceedings: *Fabrication of Particulate Reinforced Metal Composites*, Montreal, Canada, 1990, pp. 139-144.

17. Gallagher P.K., *Materials Science and Technology, a comprehensive treatment,* eds. R.W. Cahn, P. Haasen and E.J. Kramer, Vol. 2A, 1992, pp. 511-522.

18. Chen S.P., Mussert K.M. and Van der Zwaag S., Precipitation Kinetics in Al6061 and an Al6061-alumina Particle Composite, *Journal of materials Science*, Vol. 33, 1998, pp. 4477-4483.

19. Vossenberg M.S., *A Differential Scanning Calorimetry study on the influence of aging treatments on the precipitation behaviour in Al-Mg-Si alloys,* Graduation report, Delft, 1998.

20. Appendino P. and Bandini C., '6061 Aluminium Alloy-SiC Particulate Composite: a Comparison Between Aging Behaviour in T4 and T6 Treatments', *Materials Science and Engineering*, Vol. A135, 1991, pp. 275-279.

21. Das T., Munroe P.R. and Bandyopadhyay S., 'The Effect of Al_2O_3 Particulates on the Precipitation Behaviour of 6061 Aluminium-matrix Composites', *Journal of Materials Science*, Vol. 31, 1996, pp. 5351-5361.

22. Ewalds H.L. and Wanhill R.J.H., *Fracture Mechanics,* 3rd edition, Delft: Delftse Uitgevers Maatschappij, 1993, pp. 20, 95.

23. ASTM E399-90, Standard Test Method for Plane Strain Fracture Toughness of Metallic Materials", Annual Book of ASTM Standards, 1994, pp. 407-437.

24. *Duralcan Composites for Wrought Products: Mechanical and Physical Property Data,* Alcan, Canada.

25. Brooks C.R. and Choudhury A., *Metallurgical Failure Analysis*, New York, MacGraw-Hill, Inc, 1993, pp. 141-143.

26. Wei L. and Huang J.C., 'Influence of Heat Treatment and Hot Working on Fracture Toughness of Cast Aluminium Base Composites', *Materials Science and Technology*, Vol. 9, 1993, pp. 841-852.

27. Mummery P. and Derby B., 'The Influence of Microstructure on the Fracture Behaviour of Particulate Metal Matrix Composites', *Materials Science and Engeneering,* Vol. A135, 1991, pp. 221-224.

28. Hadianfard M.J., Healy J.C., and Mai Y.W., 'Fracture Characteristics of a Particulate-reinforced Metal Matrix Composite', *Journal of Materials Science,* Vol. 29, 1994, pp. 2321-2327.

29. Klimowicz T.F., and Vecchio K.S., 'The Influence of Aging on the Fracture Toughness of Alumina-Reinforced Aluminium Composites', *Fundamental Relationships Between Microstructure & Mechanical Properties of Metal-Matrix Composites,* eds. P.K. Liaw. and M.N. Gungor, 1990, pp. 255-267.

30. Shyong J.H. and Ruiz C., 'The Relationship Between Microstructure and Deformation of SiC Particulate Reinforced Al-6061', *International Conference on Advanced Composite Materials 1993*, eds. T. Chandra and A.K. Dhingra, 1993, pp. 1055-1060.

31. Dutta I. and Majumdar B.S., 'Effect of Processing on the Fracture Characteristics of a 6092 Al Composite Reinforced with SiC_p', *Materials Science Forum,* Vol. 217-222, 1996, pp. 1473-1478.

32. ASTM E 8M-94a,'Standard Test Methods for Tension Testing of Metallic Materials [Metric]', Annual Book of ASTM Standards, Vol. 14.02, 1994, pp. 81-100.

33. Jablonski D.A., Journet B., Vecchio R.S., and Hertzberg R., 'Compliance functions for various fracture mechanics specimens', *Engineering Fracture Mechanics,* Vol. 22, 1985, pp. 819-823.

34. Wang J., Furukawa M., Horita Z., Nemoto M., Ma Y. and Langdon T.G., 'The Age-Hardening Characteristics of an Al-6061/Al_2O_3 Metal Matrix Composite', *Metallurgical and Materials Transactions A,* Vol. 26A, 1995, pp. 581-587.

35. Strangwood M., Hippsley C.A. and Lewandowski J.J., 'Interfacial Segregation in Al based Metal Matrix Composites', *Low Density, High Temperature Powder Metallurgy Alloys,* eds. W.E. Frazier, M.J. Koczak and P.W. Lee, 1991, pp. 97-107.

36. Hascaryantono A.P., 'Plane-Strain Fracture Toughness Test of Aluminium Alloy AA6061 in Various Heat Treatment Conditions', practical work report, Delft, 1999

37. Dowling J.M., and Martin J.W., 'The Influence of Mn Additions on the Deformation Behaviour of an Al-Mg-Si Alloy', *Acta Metallurgica*, Vol. 24, 1976, pp. 1147-1153.

38. Chadwick R., Muir N.B. and Grainger H.B., 'The Effect of Iron, Manganese and Chromium on the Properties in Sheet Form of Aluminium Alloys Containing 0.7% Magnesium and 1.0% Silicon', *Journal of the Institute of Metals*, Vol. 82, 1953-54, pp. 75-80.

39. Prince K.C. and Martin J.W., 'The Effects of Dispersoids upon the Micromechanisms of Crack Propagation in Al-Mg-Si Alloys', *Acta Metallurgica*, Vol. 24, 1979, pp. 1401-1408.

40. Kaufman J.G., 'Experience in Plane-strain Fracture Toughness Testing per ASTM Method E399', *Developments in Fracture Mechanics Test Methods Standardisation, ASTM STP 632*, W.F.Brown Jr and J.G. Kaufman, American Society for testing Materials, 1977, pp. 3-24.

41. Liebowitz H. and Efis J., 'On Nonlinear Effects in Fracture Mechanics', *Engineering Fracture Mechanic*, Vol. 3, 1971, pp. 267-281.

42. Mussert K.M., Janssen M., Bakker A. and van der Zwaag S., 'Modelling Fracture Behaviour of an Al_2O_3 Particle Reinforced AA6061 Alloy', *Progress in Mechanical Behaviour of Materials, Proceedings of the Eight International Conference on the Mechanical Behaviour of Materials ICM 8*, eds. F. Ellyin and J.W. Provan, 1999, pp.835-839.

Dankwoord

Tijdens mijn afstuderen heb ik hulp gehad van vele mensen op vele manieren. Ik kan niet al die mensen hier opsommen maar er zijn er een paar die ik hier wil noemen.
Allereerst wil ik Katja Mussert bedanken voor haar dagelijkse begeleiding, advies en gezelligheid gedurende de ruim 2 jaar dat zij mijn begeleidster is geweest.
Dan wil ik Micheal Janssen, Ad Bakker, Sybrand van der Zwaag en Russell Wanhill bedanken voor hun uitleg en hulp bij praktische of theoretische problemen.
Adirakhmantyo Hascaryantono wil ik bedanken voor het doen van proeven waarvan ik de resultaten heb gebruikt.
Het maken van proefstukken van het mmc is lastig en zou onmogelijk geweest zijn zonder de hulp van de Instrumentmakerij en André Hoogstrate.
Het afstuderen was en bleef gezellig dankzij de vakgroep, medestudenten en medewerkers door heel het gebouw van Materiaalkunde, bedankt voor de gezelligheid.
Als laatste wil ik mijn familie en vrienden bedanken want zoals bij alle andere dingen in mijn leven stonden ze ook altijd voor mij klaar tijdens mijn afstuderen.

APPENDIX 1

A graph from the x-y plotter connected to the thermocouple. It was recorded during B heat treatment of the AA6061 tensile specimens. The graph starts when the specimen is kept at 80 °C, and the arrow indicates the point where heating at a rate of 5 °C/min was started. The specimens were quenched when 256 °C was reached.

APPENDIX 2

The Instron 4505 testing machine used for the tensile and K_{Ic} tests.